JOURNAL OF GEOPHYSICAL RESEARCH, VOL. 93, NO. B6, PAGES 6369–6396, JUNE 10, 1988

Constraining Aspherical Structure With Low-Degree Interaction Coefficients: Application to Uncoupled Multiplets

MICHAEL RITZWOLLER,[1] GUY MASTERS, AND FREEMAN GILBERT

Institute of Geophysics and Planetary Physics, University of California, San Diego, La Jolla

The effect of even-order aspherical structure on displacement for each isolated multiplet in the Earth's seismic free oscillation spectrum can be represented by a discrete set of coefficients which characterize the interaction between singlets. Each interaction coefficient is linearly related to aspherical structure of a given harmonic degree and azimuthal order. Although interaction coefficients are nonlinearly related to displacement, they can be estimated iteratively by Newton's method, a technique that we call spectral fitting. We have applied spectral fitting to approximately 350 recordings taken from 18 large or deep events and have estimated the degrees 2 and 4 interaction coefficients for 38 low harmonic degree ($\ell \leq 9$) multiplets. An error analysis, based on misfit, is also presented. These coefficients and errors provide linear constraints on aspherical structure and are tabulated for use in future inversions. The estimated coefficients partition naturally into two subsets: those for the 10 anomalous multiplets and those for the 28 multiplets dominantly sensitive to mantle heterogeneity. On average, the degree 4 coefficients lie below the error estimates, and we interpret only the degree 2 coefficients. The degree 2 coefficients for the mantle sensitive multiplets behave smoothly, within observational error, along low radial order dispersion branches (${}_0S$, ${}_1S$, ${}_2S$, ${}_5S$), indicating that a simple mantle model exists that will fit them. Comparison between the estimated interaction coefficients and those predicted by models expressed as perturbations to v_s or v_p is complicated by the necessity of assuming empirical scaling relationships between v_s, v_p, and ρ. The numerical values in these relationships are currently subject to debate, but in any reasonable case the degree 2 coefficients predicted from the models M84A and L02.56 of Dziewonski and Woodhouse agree qualitatively with the estimated coefficients. A wide range of mantle models will quantitatively fit the mantle sensitive coefficients, the fundamental mode coefficients computed from multiplet center frequency observations (${}_0S_{20} - {}_0S_{40}$), and the geoid simultaneously. The characteristics of these models are strongly dependent on allowed model characteristics with trade-offs between volumetric and boundary perturbations being particularly important. In agreement with the results described in an earler paper using a different technique, the anomalous multiplets are dominated by degree 2, axisymmetric structure somewhere in the core. Inferences concerning the nature and location of this heterogeneity are also dependent upon the scaling relationships and constraints placed on mantle structure. Not surprisingly, the resolution of the cause of anomalous splitting awaits confidence in long-wavelength mantle models and more and different kinds of data.

1. INTRODUCTION

Digital seismic data from the International Deployment of Accelerometers and the Global Digital Seismic Array have been accumulating for more than a decade and have stimulated observational studies of the aspherical structure of the Earth. The aim of the present study is to provide new constraints on long-wavelength aspherical structure by using information contained in these low-frequency seismic recordings. Aspherical structure manifests itself at low frequencies by splitting and coupling the singlets from one or more multiplets. Perturbations of the Earth from spherical symmetry split singlet frequencies which would be degenerate if the symmetry were intact. Such splitting dominantly affects spectra by producing phase shifts relative to the spherically symmetric reference state. Coupling between singlets, either within a multiplet or between multiplets, can further produce large-amplitude perturbations. Both of these effects are observationally well documented and are becoming better understood. *Masters et al.* [1982] observed fundamental spheroidal mode frequency shifts analogous to phase shifts to Rayleigh wave packets and used the formalism of *Jordan* [1978] (a theory of great circular averages asymptotically valid for large harmonic degree ℓ) to interpret these observations in terms of spherical harmonic degree 2 lateral heterogeneity in the transition zone. *Woodhouse and Dziewonski* [1984] developed a technique, based on the same asymptotic formalism, which used the phase shifts in the time domain to produce aspherical models of the upper mantle with degrees 1–8. *Davis and Henson* [1986] recently studied the domain in which the great circle average approximation is valid. *Davis* [1987] reanalyzed the center frequency data used by *Masters et al.* [1982] with a more accurate theory, and *Smith et al.* [1987] analyzed a somewhat larger center frequency data set with a fully nonasymptotic theory. *Masters et al.* [1983] observed perturbations to the degenerate frequencies and attenuation rates of fundamental spheroidal and toroidal modes due to coupling caused by the Coriolis force. Direct observations of the singlet frequencies of a number of low harmonic degree multiplets were reported by *Ritzwoller et al.* [1986]. All these studies concentrated on interpreting perturbations in phase caused by aspherical structure. A more nearly complete use of long-period data would include amplitude information as well.

This study presents the systematic application of one such technique, which we call iterative spectral fitting [*Ritzwoller et al.*, 1986], to a number of low harmonic degree multiplets which are believed to be no more than weakly coupled to other nearby multiplets. As will be described in section 2, the effect of even-order aspherical structure on displacement for each uncoupled multiplet can be represented by a set of discrete complex coefficients, each linearly related to aspherical structure of a given degree and order. Since these coefficients are linearly related to aspherical structure, *Ritzwoller et al.* [1986] referred to them as aspherical structure

[1]Now at Department of Earth and Planetary Sciences, Harvard University, Cambridge, Massachusetts.

Paper number 7B5038.
0148-0227/88/007B-5038$05.00

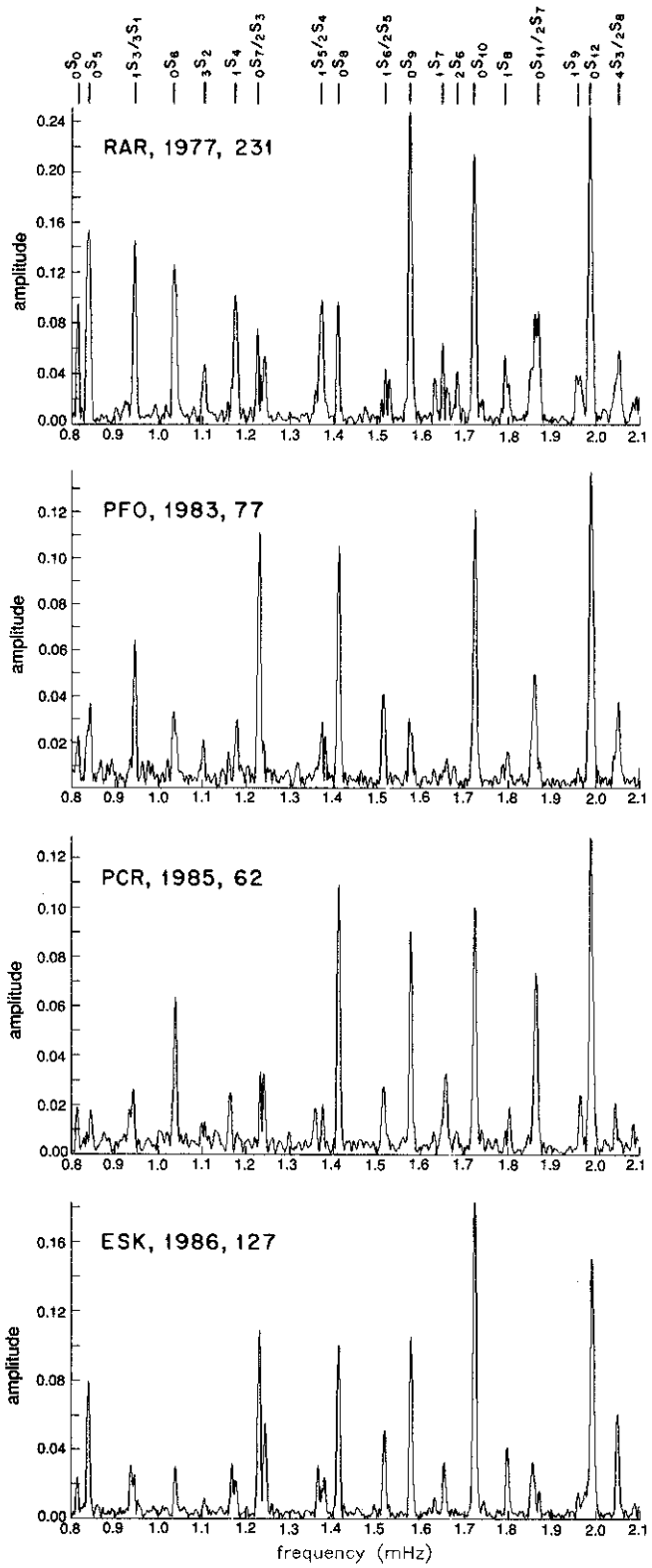

Fig. 1. High signal-to-noise amplitude spectra of four 75-hour records, from different events, exhibiting low harmonic degree overtones.

coefficients. This name is potentially confusing since it may also be used for the model coefficients which represent aspherical structure. *Woodhouse et al.* [1986] and *Giardini et al.* [1987] refer to the coefficients, when multiplied by the corresponding spherical harmonics and summed, as splitting functions. This name underscores the primary role that they play in determining the structure of the splitting matrix. Since these coefficients control general singlet interactions and not just frequency splitting, we choose now to call them interaction coefficients. (Splitting coefficients are the coefficients which govern the frequency splitting caused by the Coriolis force, centripetal acceleration, and ellipticity of figure [*Dahlen and Sailor*, 1979].) Furthermore, we wish to generalize the technique to be applicable to coupled multiplets, in which case the splitting matrix is usually called the interaction matrix.

The interaction coefficients can be estimated by iterative spectral fitting, the goal of which is to improve iteratively the coefficient estimates by minimizing the spectral residual, the difference between a synthetic spectrum and the data spectrum for a given multiplet within a specified frequency band:

$$\min \sum_n \int_{\omega_{\min}}^{\omega_{\max}} w_n(\omega)\Delta s_n(\omega)d\omega$$

where Δs is the residual spectrum, n is the recording index, and w_n is a weight which will be discussed later. To the best of our knowledge this technique was first vaguely referred to by *Ritzwoller and Masters* [1984], but a very similar technique was developed independently and the first results were reported by *Woodhouse and Giardini* [1985]. Further results from the application of this technique are given by *Ritzwoller et al.* [1986], *Woodhouse et al.* [1986], and *Giardini et al.* [1987].

We applied this algorithm, which is described in detail in section 2, to approximately 350 recordings from 18 large events and estimated the degrees 2 and 4 interaction coefficients for 38 multiplets. Once estimated, these coefficients provide integral constraints on aspherical structure and can, in principle, be used as data in the inversion for the causative structure. Unlike studies which concentrate on fundamental modes, many of the multiplets we consider are very sensitive to structure below the upper mantle, and the coefficients we estimate constrain aspherical structure at all radii. As Figure 1 exhibits, there have been a number of large earthquakes which excite these multiplets in the last few years, and the quantity and quality of data are now adequate to perform the experiments described herein.

The technique breaks naturally into two parts: a discrete regression for the interaction coefficients for a number of multiplets (spectral fitting) followed by a continuous inverse problem. We present a first step in the construction of a catalogue of coefficients which constrain aspherical structure throughout the entire Earth. The coefficients presented here are insufficient to resolve even the degree 2 part of mantle structure unambiguously. However, they do provide new tests on existing mantle models (see section 4.1) and can be used in future inversions with similar or quite different kinds of data than used here. It is interesting to consider the range of models which will fit the estimated coefficients. For this reason we present the result of an inversion for degree 2 mantle structure using a method of inversion (see the appendix) quite different from that used in previous inversions for aspherical mantle models (in particular, the reference models M84 of *Woodhouse and Dziewonski* [1984] and LO2.56 of *Dziewonski* [1984]). Instead of choosing a set of smooth basis functions a priori, we follow *Gilbert et al.* [1973] and explicitly solve for smooth models between seismic discontinuities by minimizing the sum of the integral of the square of the radial second derivative of the volumetric perturbations and the square of the Euclidean norm of the boundary perturbations.

We attempt to limit discussion to multiplets which, to a good approximation, can be considered uncoupled, and the accuracy of the coefficient estimates depends critically on the judicious choice of multiplets analyzed. We have concentrated on isolated multiplets mainly as a computational convenience, but this focus has the unfortunate consequence of constraining only the even-order part of aspherical structure. However, the generalization of spectral fitting to coupled multiplets is straightforward and will greatly expand the data set by including multiplets of higher harmonic degrees. In principle, it will also allow constraints to be placed on odd-order heterogeneity, although as discussed by *Masters and Ritzwoller* [1987], the effect of long-wavelength odd-order structure on the data is slight. This will be the subject of a later paper.

Attempts to model low-frequency seismic data with great precision hold promise for geological and geodynamical relevance, albeit on a global scale [*Jarvis and Peltier*, 1986]. Aspherical effects have been observed in a number of body wave phases which sample the lower mantle and core-mantle boundary (CMB) [*Doornbos*, 1983; *Lay*, 1987]. Travel times from the huge International Seismological Centre (ISC) data set have been used in tomographic inversions to try to map the longest wavelengths of aspherical structure in the lower mantle [*Clayton and Comer*, 1983; *Dziewonski*, 1984]. Although the models produced by these two studies are qualitatively similar at degree 2, they differ in amplitude by about a factor of 2 (R. W. Clayton, personal communication, 1987). Further constraints on the lower mantle from low-frequency seismic data should help resolve this disagreement, but as will be described shortly, these efforts are troubled by difficulties in comparing body wave and free oscillation models which also translate into ambiguities in amplitude. Recent studies of the anomalous travel times of *PKP* phases [*Poupinet et al.*, 1983; *Morelli and Dziewonski*, 1987; *Creager and Jordan*, 1986*b*] and the anomalous splitting of multiplets in the Earth's free oscillation spectrum which is very sensitive to the core [*Masters and Gilbert*, 1981; *Ritzwoller et al.*, 1986; *Giardini et al.*, 1987] seem to point to the existence of large-scale, dominantly axisymmetric heterogeneity on or below the CMB. It is not unlikely that the cause of these disparate phenomena are related, but investigators have not yet been able to agree on the nature or location of the causative structure(s). *Ritzwoller et al.* [1986] presented the simplest smooth model of aspherical structure in the core which fits most of the free oscillation data. To date, a number of seriously proposed hypotheses have been entertained, including large-amplitude structure on the CMB [*Creager and Jordan*, 1986*b*; *Morelli and Dziewonski*, 1987] and/or inner core boundary (ICB) [*Poupinet et al.*, 1983; *Giardini et al.*, 1987], a chemical boundary layer above or below the CMB [*Creager and Jordan*, 1986*b*], large isotropic volumetric perturbations in the inner core [*Giardini et al.*, 1987], and anisotropy in the inner core [*Woodhouse et al.*, 1986; *Morelli et al.*, 1986]. It remains unclear which, if any, of these features are physically plausible. It is clear that it will only be through the application of a number of different techniques with data which span the seismic frequency band which will allow us to infer any one of the competing alternatives.

A natural approach to improve constraints on the lower mantle and core is to attempt to combine body wave and free oscillation data sets and to interpret them jointly [*Woodhouse and Dziewonski*, 1986]. Meaningful comparisons between models independently produced by body wave and free oscillation studies are difficult. Although free oscillation data are sensitive to both shear velocity v_s and compressional viscosity v_p, as well as density ρ, the data are currently insufficient to estimate simultaneously all three functions of radius for each degree and order of aspherical structure. As described in the appendix, a common approach has been to assume an empirical linear scaling relationship between relative perturbations in v_s, v_p, and ρ, reducing the problem to the estimation of a single function of radius in any one of the three variables. The relationships used in the present paper are $d \ln v_p / d \ln \rho$ and $d \ln v_s / d \ln v_p$. As described in the appendix, the numerical values of these relationships affect the amplitude of the integral kernel in the definition of the interaction coefficients. Uncertainties in these values will result in ambiguities in the amplitude of the inferred model and hence will exacerbate comparison between free oscillation and body wave models.

The motivation for the linear scaling approach has been the observation of the near constancy of the ratios of the temperature derivatives of the relative quantities $\ln\kappa$, $\ln\mu$, $\ln v_s$, and $\ln v_p$ for many materials (κ and μ are the bulk and shear moduli, respectively). For example, *Chung* [1971] determined the temperature derivative of various olivine compositions and estimated that $d \ln v_s / d \ln v_p \sim 1.3$. In addition, it is easy to show that if partial melt were the sole cause of lateral variations and if it were to affect just μ while κ and ρ were fixed, then $d \ln v_s / d \ln v_p \sim 2.25$. Obviously, the appropriate values that the scaling relationships are to take, if in fact they are relevant to the Earth, are dependent on the nature of the lateral heterogeneity. It is not unlikely that lateral heterogeneities result from some combination of temperature variations, partial melting, and chemical heterogeneities. It remains an open question as to the relative importance of these contributions. If chemical heterogeneities dominate, then the linear scaling approach would probably be unfruitful. If some combination of thermal effects and partial melting dominates, then appropriate local scaling relationships probably do exist; although the values taken by these relationships will be dependent on the relative importance of these two factors, which may be a strong function of depth and may itself vary laterally.

In principle, it is straightforward to constrain $d \ln v_s / d \ln v_p$ with seismic data. Compressional and shear wave travel time residuals (δt_p and δt_s) computed as station corrections have been used both on a global scale [e.g., *Hales and Doyle*, 1967; *Orcutt et al.*, 1986] and regionally [e.g., *Romanowicz and Cara*, 1980; *Souriau and Woodhouse*, 1985] to estimate this ratio. It is easy to show, from Fermat's principle, that

$$\frac{d \ln v_s}{d \ln v_p} = \left[\frac{v_s}{v_p} \right] \frac{\delta t_s}{\delta t_p}$$

Thus, for a Poisson solid, a residual ratio $\delta t_s / \delta t_p \sim 2.2$ would agree with the thermally induced ratio $d \ln v_s / d \ln v_p \sim 1.3$, and $\delta t_s / \delta t_p \sim 4.0$ would agree with the partial melting ratio $d \ln v_s / d \ln v_p \sim 2.3$. Global residual ratios range from highs near 4.0 to the more recently determined values of 2.8–3.0 by *Orcutt et al.* [1986]. The utility of the global residual ratios has been questioned by *Romanowicz and Cara* [1980], who show how they can be biased high by neglecting the effects of tectonic regions. *Romanowicz and Cara* [1980] and *Souriau and Woodhouse* [1985] agree that the residual ratios show strong lateral variations. It is also not unlikely that the ratios are depth dependent, and studies based on station corrections probably only bear on the scaling relationships in the upper mantle. *Jordan and Lynn* [1974] compute the travel time residuals for the differential phases *ScS–S* and *PcP–P*, which agree with the global average of *Orcutt et al.* [1986] and which they localize in the top of the lower mantle. Little evidence about scaling in the deeper mantle exists. *Giardini*

et al. [1987] point out that by using $d \ln v_s / d \ln v_p > 2.0$, they can improve the fit of the model L02.56 [*Dziewonski*, 1984] to the interaction coefficients (their splitting functions). In section 4 we show that this improvement in fit is confined to a very few coefficients and can also be accomplished by a CMB perturbation. Due to the insensitivity of body wave models to density, little seismic evidence exists to constrain $d \ln v_p / d \ln \rho$. B. H. Hager and R. W. Clayton (unpublished manuscript, 1986) estimate this ratio by scaling Clayton and Comer's lower mantle model to fit the geoid.)

Thus no clear concensus has been reached on any of the scaling relationships other than perhaps that they vary laterally and that the hope of finding a useful global average may be faint. We are forced to assume linear scaling relationships in the present study, but when considering preexisting body wave models, as in section 4, we consider the values mentioned above as end-members in a suite of physically realistic alternatives and report comparisons from both end-members.

Following a brief discussion of the forward problem for isolated multiplets, we describe spectral fitting in some detail. The data analysis is discussed in section 3 with emphasis placed on the analysis of misfit. A comparison between the estimated interaction coefficients and those computed from existing mantle models and the inverse problem for degree 2 structure are included in section 4. We focus on problems associated with inferring mantle structure, but the interpretation of the anomalous multiplets is also briefly discussed.

2. Theoretical Preliminaries

2.1. *First-Order Splitting Theory*

Consider a set of multiplets, represented by the index $k = (n, \ell)$, which for some reason can be considered approximately uncoupled (e.g., they may be isolated in complex frequency or may not satisfy the angular selection rules). Here n and ℓ are the radial order and harmonic degree of each multiplet k. A complete description of the effect of small general aspherical perturbations on uncoupled multiplets is given by *Woodhouse and Dahlen* [1978] and *Woodhouse and Girnius* [1982]. These results frequently are called first-order splitting theory which we merely summarize here.

The displacement field at spherical polar position $\mathbf{r} = (r, \theta, \phi)$ excited by a point source at $\mathbf{r}_0$ with moment rate tensor $\mathbf{M}$ can be written as the inner product

$$\mathbf{s}(\mathbf{r},t) = \mathrm{Re}\left\{ \sum_k \boldsymbol{\sigma}_k(\mathbf{r}) \cdot \mathbf{a}_k(\mathbf{r}_0,t) e^{i\omega_k t} \right\} \tag{1}$$

where the complex envelope function vector $\mathbf{a}_k(t)$ is given by

$$\mathbf{a}_k(t) = \mathbf{P}_k(t)\mathbf{a}_k, \quad \mathbf{a}_k(0) = \mathbf{a}_k \tag{2}$$

$\mathbf{P}_k(t) = \exp(i\mathbf{H}_k t)$ is the matrizant or propagator matrix of the following first-order propagator equation with initial condition given in (2):

$$\frac{d}{dt}\mathbf{a}_k(t) = i\mathbf{H}_k\mathbf{a}_k(t) \tag{3}$$

The receiver vector $\boldsymbol{\sigma}_k$ in (1) is composed of the $2\ell+1$ singlet eigenfunctions:

$$\begin{aligned} \boldsymbol{\sigma}_k^m(r) = \hat{r}U_k(r)Y_\ell^m(\theta,\phi) &+ V_k(r)\nabla_1 Y_\ell^m(\theta,\phi) \\ &- W_k(r)\hat{r}\times\nabla_1 Y_\ell^m(\theta,\phi) \end{aligned} \tag{4}$$

The excitation vector $\mathbf{a}_k$ comprises the $2\ell+1$ excitation coefficients $a_k^m = \mathbf{M} : \boldsymbol{\varepsilon}_k^{m*}(\mathbf{r}_0)$. The term $\boldsymbol{\varepsilon}_k^{m*}$ is the complex conjugate of the strain tensor for the azimuthal order m singlet and is expressible in terms of the multiplet scalars U_k, V_k, and W_k in (4) [*Gilbert and Dziewonski*, 1975]. The complex spherical harmonics, Y_ℓ^m, are normalized according to the convention of *Edmonds* [1960].

The dependence of displacement on aspherical structure in (1) can be made explicit by considering the components of the $(2\ell+1)\times(2\ell+1)$ complex splitting matrix $\mathbf{H}_k$:

$$H_{mm'}^k = \omega_k(a_k + mb_k + m^2c_k)\delta_{mm'} + \sum_{\substack{s=2 \\ \text{even}}}^{2\ell} \gamma_s^{mm'}{}_k c_s^{m-m'} \tag{5}$$

where

$${}_k c_s^t = \int_0^a \delta\mathbf{m}_s^t(r) \cdot {}_k\mathbf{G}_s(r) r^2 dr - \sum_d^D r_d^2 h_{sd}^t \, {}_k B_s \tag{6}$$

The first term on the right-hand side of (5) represents the contribution by rotation and hydrostatic ellipticity of figure. Here ω_k is the degenerate frequency, and numerical values of the splitting parameters a_k, b_k, and c_k evaluated for some multiplets are given by *Dahlen and Sailor* [1979] and *Ritzwoller et al.* [1986]. We call the model containing only these contributions to $\mathbf{H}_k$ the RH model (standing for rotating, hydrostatic Earth model). The second term contains the additional effect of general even-order aspherical volumetric ($\delta\mathbf{m}_s^t(r)$) and boundary (h_{sd}^t) perturbations. Aspherical perturbations are represented with spherical harmonic basis functions of degree s and order t:

$$\delta\mathbf{m}(\mathbf{r}) = \sum_{s,t} \delta\mathbf{m}_s^t(r) Y_s^t(\theta,\phi) \qquad h_d(\theta,\phi) = \sum_{s,t} h_{sd}^t Y_s^t(\theta,\phi) \tag{7}$$

for each boundary d. The model vector is

$$\delta\mathbf{m}_s^t(r) = (\delta p_s^t(r), \delta\kappa_s^t(r), \delta\mu_s^t(r))^T$$

and the integral kernel vector is

$$\mathbf{G}_s(r) = (R_s(r), K_s(r), M_s(r))^T$$

where R_s, K_s, and M_s can be computed using the formulas given by *Woodhouse and Dahlen* [1978]. Each multiplet k possesses a unique set of complex interaction coefficients ${}_k c_s^t$ whose amplitude and phase are functions of the amount and distribution of heterogeneity in the Earth and of the manner in which the multiplet samples this heterogeneity. All of the other constituents of (6) can be computed analytically. Estimation of the c_s^t fully determines the splitting matrix and therefore the effect of aspherical structure on the displacement field for an isolated multiplet.

Insight into the way aspherical structure affects the displacement field is gained by a consideration of the spectral decomposition of $\mathbf{H}_k$:

$$\mathbf{H}_k\mathbf{U}_k = \mathbf{U}_k\boldsymbol{\Omega}_k \tag{8}$$

Here $\mathbf{U}_k$ is the unitary matrix whose columns are the eigenvectors of $\mathbf{H}_k$ and $\Omega_{mm'}^k = \delta\omega_k^m\delta_{mm'}$ is the diagonal matrix of eigenvalues. Equations (5) and (6) demonstrate that aspherical structure splits the singlet frequencies within each multiplet: $\omega_k^m = \omega_k + \delta\omega_k^m$. For the RH model, $\omega_k^m = \omega_k + \omega_k(a_k + mb_k + m^2c_k)$ and $\mathbf{U}_k = \mathbf{I}$. If $\mathbf{U}_k = \mathbf{I}$, the mth singlet frequency is uniquely associated with the mth element of the receiver and excitation vectors. In this case, each envelope function $a_k^m(t)$ in (1) is a pure harmonic time function. Additional aspherical structure further splits the singlet frequencies and perturbs $\mathbf{U}_k$ from $\mathbf{I}$, producing cross-azimuthal coupling which associates more than one element of the receiver and exci-

tation vectors with each singlet frequency. Thus $a_k^m(t)$ becomes a sum of single harmonics displaying a more complicated temporal behavior caused by the interchange of energy among azimuthal orders. Since the apparent period of the envelope function is controlled by the singlet frequency perturbations in $\mathbf{\Omega}_k$, which are relatively small, $a_k^m(t)$ will be very slowly varying in time.

2.2. *Estimating the Interaction Coefficients*

Examination of (1) shows that it is the envelope functions $a_k^m(t)$ which provide the raw material that must be used to constrain aspherical structure. In the time domain the envelope functions for a single multiplet cannot be separated easily from those of other multiplets. However, in the frequency domain where aspherical structure produces spectral amplitude and phase shifts, many multiplets are isolated. These two effects can be seen easily in Figure 2 in which we compare data and synthetic spectra for ${}_{13}S_2$ calculated with the RH model (dotted lines) and the degrees 2 and 4 interaction coefficients listed in Table 3 (dashed lines). As pointed out by *Ritzwoller et al.* [1986], the RH model very poorly fits anomalous multiplets such as ${}_{13}S_2$. However, Figure 2 shows that the fit to the data can be greatly improved both in amplitude and phase by using the interaction coefficient estimates in Table 3. (Phase can only be well fit near spectral peaks; disagreement in phase in low-amplitude regimes is dominated by noise.) Since ${}_{13}S_2$ is anomalously split, the perturbation to the spectrum caused by aspherical structure is unusually large. Figure 2 demonstrates the effect of aspherical structure for the normally split multiplet ${}_0S_6$. The improvement in fit to this multiplet is dominated by improvement in phase, as the spectra for CMO and GAR in Figure 2 exhibit. Clearly, in either case, the amount of signal is quite large.

Since the interaction coefficients ${}_k c_s^t$ are, by (6), linearly related to aspherical structure, the accurate estimation of the coefficients for many multiplets results in a linear inverse problem for the perturbing structure: $\delta\mathbf{m}(\mathbf{r})$ and $h_d(\theta,\phi)$. Unfortunately, as (1), (2), (5), and (6) show, the ${}_k c_s^t$ are nonlinearly related to displacement. *Ritzwoller et al.* [1986] showed that the ${}_k c_s^t$ can be estimated by Newton's method. Fixing k, this technique is based on the linearization of the dependence of displacement on small perturbations in the interaction coefficients δc_s^t and complex degenerate frequency $\delta\omega_k$:

$$\mathbf{s}(\mathbf{r},t) \approx \mathbf{s}_o(\mathbf{r},t) + \sum_{s,t} \frac{\partial \mathbf{s}_o(\mathbf{r},t)}{\partial c_s^t}\,\delta c_s^t + \frac{\partial \mathbf{s}_o(\mathbf{r},t)}{\partial \omega_k}\,\delta\omega_k \qquad (9)$$

Here $\mathbf{s}_o(\mathbf{r},t)$ is the displacement field at the reference c_s^t values. The partial derivative $\partial\mathbf{s}/\partial\omega_k$ is trivially calculated from (1). *Ritzwoller et al.* [1986] (see the appendix) presented two techniques for analytically computing the partial derivatives $\partial\mathbf{s}/\partial c_s^t$. The first involved a recurrence relation in time and is the technique used in this paper. However, such recursive algorithms are nonoptimal for vector mode computers. The second technique was a nonrecursive algorithm based on an inhomogeneous propagator formalism. Both techniques are designed to create derivative seismograms in the time domain to which data gaps are then added and tapers applied and which are finally Fourier transformed.

After Fourier transforming (9), define the spectral residual for the n th recording at iteration j as

$$\Delta\mathbf{s}_n^{(j)}(\mathbf{r},\omega) = \mathbf{s}_n(\mathbf{r},\omega) - \mathbf{s}_{o_n}^{(j)}(\mathbf{r},\omega) \qquad (10)$$

where $1 \le n \le N$. Discretize frequency $\omega_i \in [\omega_{\min},\omega_{\max}]$ with $1 \le i \le I$, let $\delta c_P = \delta\omega_k$, and rewrite (9) as

$$\Delta\mathbf{s}_n^{(j)}(\omega_i) = \sum_{p=1}^{P} \frac{\partial \mathbf{s}_n^{(j)}(\omega_i)}{\partial c_p}\,\delta c_p = \sum_{p=1}^{P} A_{nip}^{(j)}\delta c_p \qquad (11)$$

where c_p is one of the c_s^t with $1 \le p \le \frac{1}{2}s_{\max}(s_{\max}+3)+1 = P$ and where $s_{\max}$ is the maximum degree of the even-order aspherical structure specified. For simplicity, (11) can be rewritten as the incremental matrix equation

$$\Delta\mathbf{s}^{(j)} = \mathbf{A}^{(j)}\delta\mathbf{c} \qquad (12)$$

Each frequency component forms a different row of the residual vector $\Delta\mathbf{s}$ and the partial derivative matrix $\mathbf{A}$. Each column of $\mathbf{A}$ represents the contribution from a unique degree and order of aspherical structure, i.e., a single p value. Contributions from subsequent recordings are stacked vertically in $\Delta\mathbf{s}$ and $\mathbf{A}$. We write the solution to (12) (the incremental normal equtions) symbolically as

$$\delta\mathbf{c} = \mathbf{A}^{-1}\Delta\mathbf{s} \qquad (13)$$

The generalized inverse can be obtained with the SVD algorithm of *Golub and Reinsch* [1971]. The algorithm represented by (9)–(13) is simply a Newton's method solution to the nonlinear problem.

The estimator defined by (13) is extremely sensitive to statistical outliers. Outlier resistance, or robustness, can be improved in a number of standard ways [*Huber*, 1981]. We have found a simple row weighting scheme, based on the residual level at each recording to be useful. We define the row weight to be applied to the rows of $\Delta\mathbf{s}$ and $\mathbf{A}$ belonging to the n th recording on iteration j as

$$w_n^j = \left[(1/I) \sum_{i=1}^{I} (\Delta s_n^j(\omega_i))^2 \right]^{-1/2} \qquad (14)$$

(This is simply the inverse rms residual computed across frequency for the n th recording.) As well as improving the stability of $\mathbf{A}$, this scheme weights down poorly fit records, desensitizing the estimator to unspecified structure, weak coupling to other multiplets, and noisy recordings. We have also found that a change in units performed by normalizing the square of the Euclidean norm of the columns of the partial derivative matrix before decomposition enhances the stability of the algorithm [*Lawson and Hanson*, 1974]. This procedure is iterated until no significant improvement in fit to the data is achieved.

The degrees 2 and 4 coefficients estimated in this way are listed in Table 3. In the event that data errors are frequency independent and the data are well fit, $1/w_n^j$ would probably be a good estimate of the standard deviation of the data error for the n th recording. In this case, if the observations are statistically independent and normally distributed, the Gauss-Markov theorem would assure us that the estimator given by (13) and (14) would be unbiased, have minimum variance, and have maximum likelihood. The coefficient covariance matrix could then be estimated in the standard way. In practice, the validity of these assumptions can only be checked by examining the residuals after fitting: they should be at the ambient noise level. Unfortunately, examination of the residuals (Figures 2–10) reveals that the data are fit imperfectly and synthetic experiments indicate that errors in the coefficient estimates due to inaccuracies in approximations and assumptions are likely to be much larger than the standard statistical estimates. In lieu of an accurate statistical model an accurate assessment of the quality of the coefficient estimates must start with an analysis

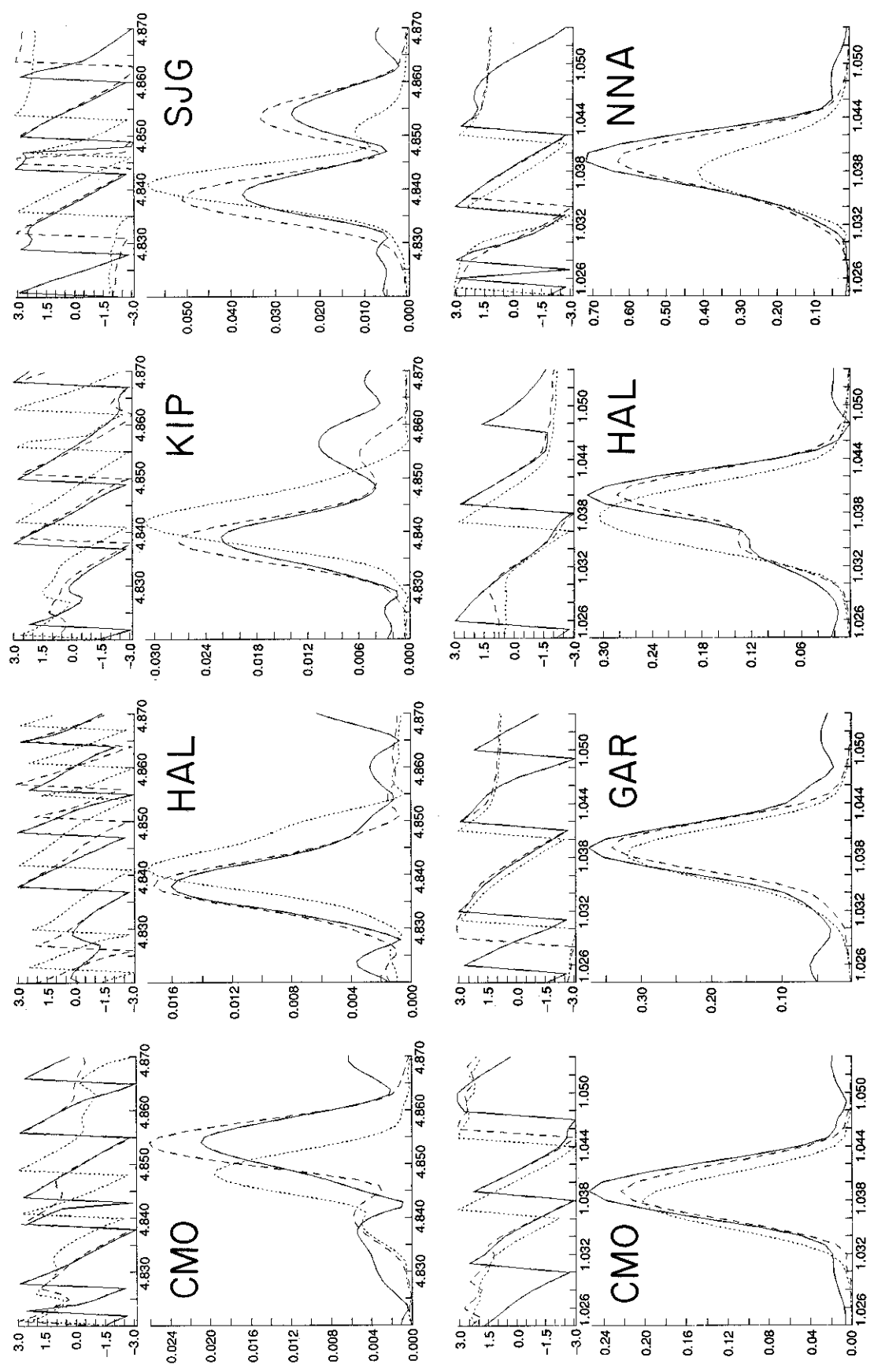

Fig. 2. (Top) Amplitude and phase spectra (solid line) of 60 hours time series for four high signal-to-noise recordings taken after the deep Banda Sea event of June 22, 1982, compared with synthetic spectra computed for ${}_{13}S_2$ relative to the estimated coefficients from Table 3 (dashed curve) and the RH model (all coefficients zero; dotted curve). Agreement in phase can only occur when peaks are above the noise as illustrated by the disagreement between synthetic and data phase away from the spectral peaks. (Bottom) Same as top, but recordings are 90 hours in length taken after the Indonesia event of August 19, 1977, and synthetics are computed for ${}_0S_6$.

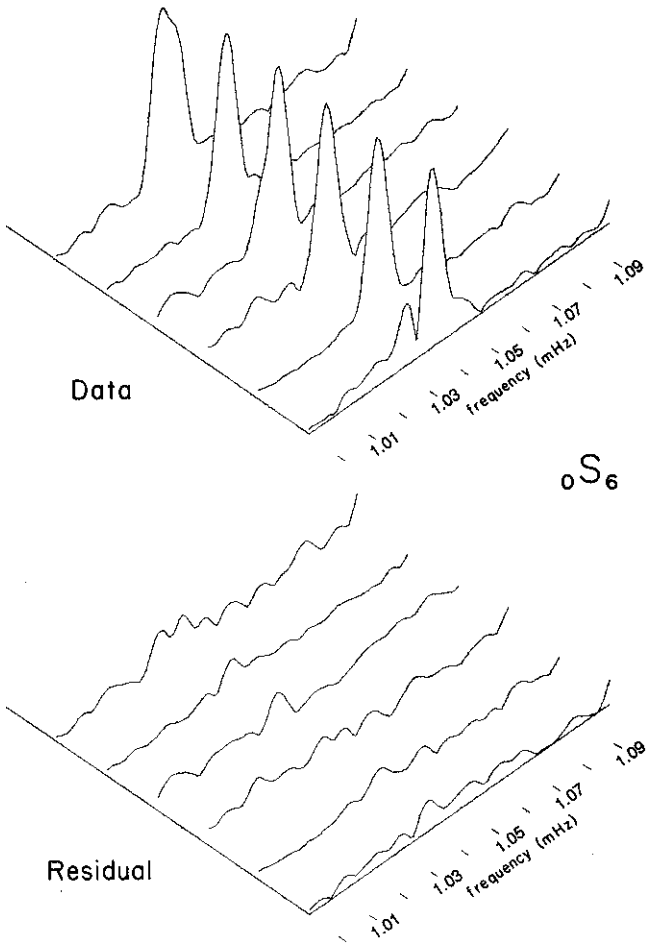

Fig. 3*a*. (Top) Amplitude spectra around ${}_0S_6$ for six high signal-to-noise recordings following the large Indonesian event on August 19, 1977. The amplitudes of the data peaks are normalized. (The four recordings shown in Figure 2 (bottom) are the second through fifth recordings here.) (Bottom) Amplitude spectra of the residuals (the difference between the data and synthetic spectra) computed with the degree 2 and 4 coefficients found in Table 3. Each residual spectrum is plotted on the same scale as the corresponding data trace.

of the cause of the misfit and its effect on the coefficients. In the next section we discuss the application of spectral fitting to 38 multiplets using a data set of more than 350 recordings from large and deep events, followed by an attempt to estimate realistically the errors in the ${}_kc_s^l$. The inversion for aspherical models from the estimated ${}_kc_s^l$ and errors is the subject of section 4.

3. Data Analysis

Spectral fitting has been applied to approximately 350 recordings taken from the Global Digital Seismic Network (GDSN) and International Deployment of Accelerometers (IDA) for the 18 earthquakes listed in Table 1. In this section we discuss the results of the application of this technique. After decisions about problem specification have been made, we address the question of whether the algorithm will converge to coefficient estimates which fit the data and whether these coefficients provide a global minimum in misfit. Systematic misfit above ambient noise is symptomatic of errors in assumptions and approximations which could lead to biased coefficient estimates. We attempt to isolate the causes of misfit and to determine their effect on the coefficient estimates. The accurate interpretation of the coefficients in terms of aspherical structure requires that coefficient error estimates reflect these effects.

3.1. *Specification and Convergence*

Since spectral fitting is both time consuming and easily degraded by noisy recordings, we use only those records with visually apparent spectral peaks. The number of recordings used for each multiplet is listed in Table 2. In general, we choose a frequency band for spectral fitting around each multiplet which overlaps the highest- and lowest-frequency singlets by about $5\,\mu$Hz. When a nearby nonoverlapping multiplet is present, we truncate the band short of the interfering multiplet. When nearly equally excited multiplets overlap in frequency (e.g., ${}_1S_5$ and ${}_2S_4$, ${}_2S_8$ and ${}_4S_3$, etc.), the coefficients for all multiplets must be estimated simultaneously. These multiplets appear as hyphenated pairs in Table 2. In principle, the definition of the ${}_kc_s^l$ in (6) includes the general effect of even-order, elastic and anelastic volumetric and boundary perturbations, and one should solve for all coefficients ($0 \le s \le 2l$). In practice, the quality, number, and distribution of data are usually insufficient to estimate all of the coefficients,

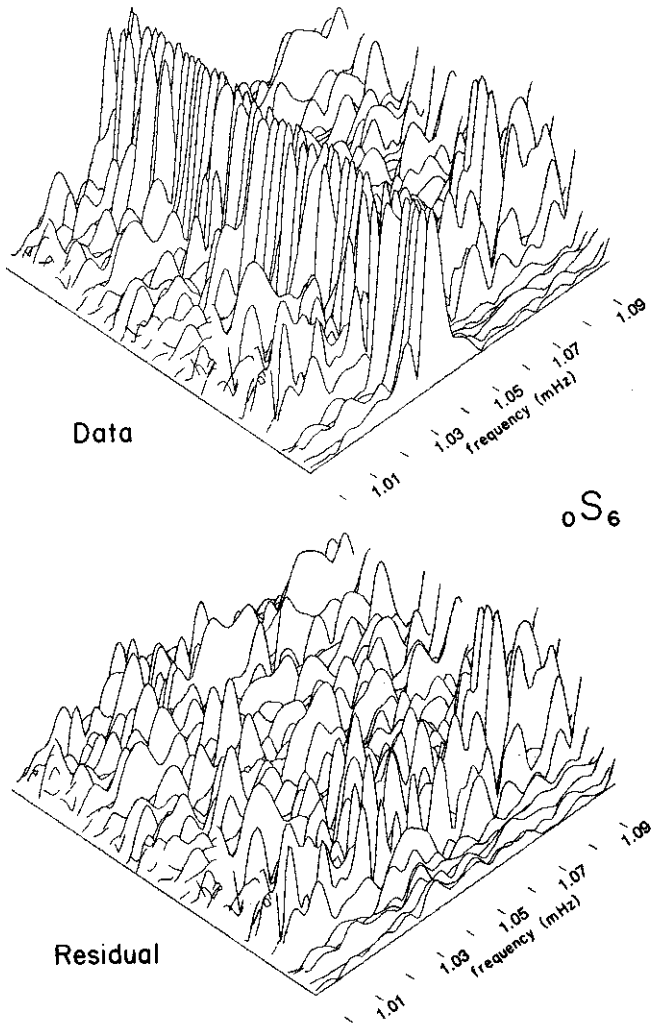

Fig. 3*b*. Same as Figure 3*a* but for 58 of the recordings of ${}_0S_6$ used in the experiment. The high signal-to-noise recordings from Figure 3*a* are plotted at the front of each plot. Recordings are plotted in no special order, although recordings from a single event are clustered.

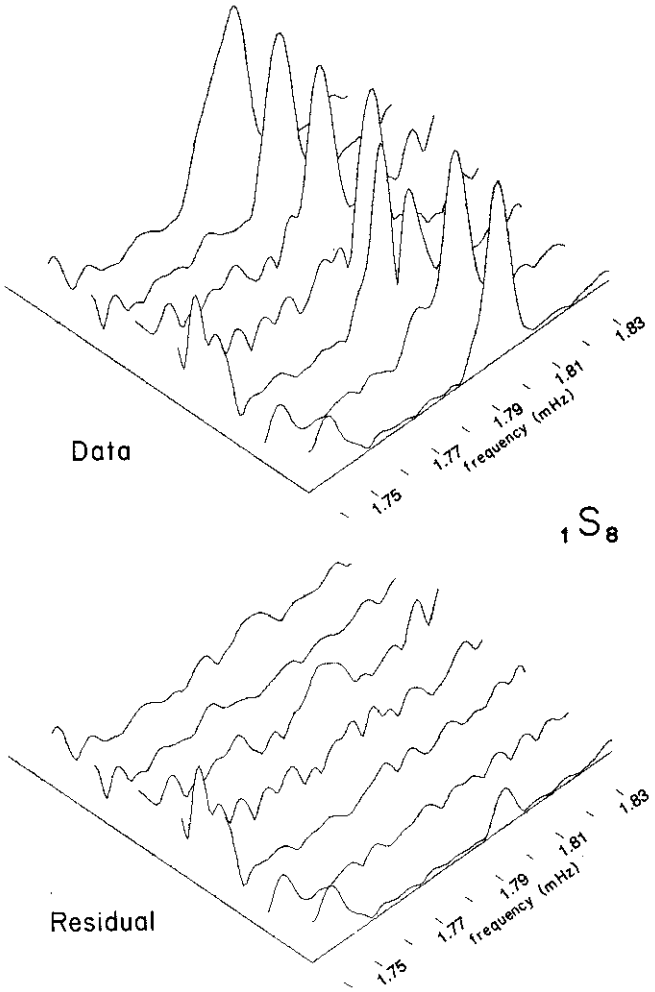

Fig. 4*a*. Same as Figure 3*a* but for seven high signal-to-noise recordings taken from several events for $_1S_8$.

even in the presence of very small amounts of noise. Once overlapping multiplets are considered, the number of coefficients doubles and problems can become formally underdetermined. We are thus forced to estimate only a subset of the coefficients for each multiplet. Since the effect of aspherical anelastic structure on the data is probably small [*Masters and Gilbert*, 1983; *Buland et al.*, 1985], we consider only aspherical elastic structure. We do estimate a perturbation in spherically averaged Q for each multiplet, i.e., a perturbation to the imaginary part of the degenerate frequency. Considering only elastic aspherical structure constrains the splitting matrix **H** to be Hermitian and the aspherical interaction coefficients to satisfy the relation $\delta c_s^{-t} = (-)^t \delta c_s^{t*}$. This nearly halves the number of degrees of freedom without significantly affecting the fit to the data. Experience shows that we can fit most genuinely isolated multiplets quite well with the degree 2 coefficients alone (see Figures 2–4). We solve for degrees 2 and 4 coefficients and list them in Table 3. The perturbing effect of unspecified structure on the estimated coefficients must then be addressed a posteriori.

We seek a robust algorithm which converges in a reasonable number of steps to accurate degrees 2 and 4 coefficient estimates. Since the algorithm is an iterative solution to a nonlinear problem, convergence to a spurious local minimum is possible. The radius of convergence of the algorithm must be determined empirically since it depends on a number of variables, among which are the multiplet under consideration, the number of recordings used, the signal-to-noise ratio, the weighting scheme, and the truncation level of the SVD. However, the most important variable is the squared Euclidean norm of the coefficient vector ($|_k c_s|^2 = \Sigma_m ({}_k c_s^m)^2$), which is a function of the magnitude of aspherical structure in the regions sampled by the multiplet. For most multiplets the norm of the coefficient vector can be bounded from above by a consideration of the multiplet's splitting width, which itself can be estimated either by examining a great many individual recordings or through singlet stripping [*Ritzwoller et al.*, 1986]. The largest coefficient norms will be possessed by the anomalous multiplets, and these cause us the greatest concern. Synthetic experiments assure us that these vectors are not outside the regime reachable by linearized iterative inversion and that for nearly all the multiplets under consideration here our algorithm possesses a radius of convergence greater than the radius of all physically realistic models. Thus problems with this estimator do not result from its nonlinear nature but reduce to problems commonly associated with the linear estimators: bias caused by unspecified structure, covariance among the estimated coefficients, etc. This does not minimize their significance.

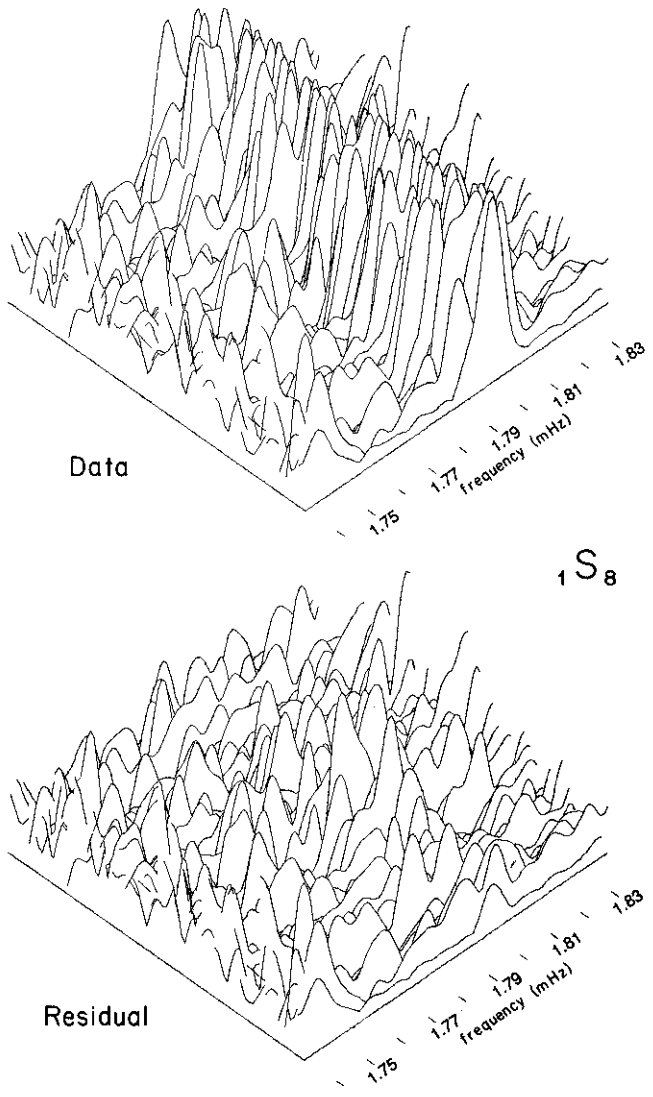

Fig. 4*b*. Same as Figure 4*a* but for 47 of the recordings used for $_1S_8$. The high signal-to-noise recordings are distributed throughout the plot.

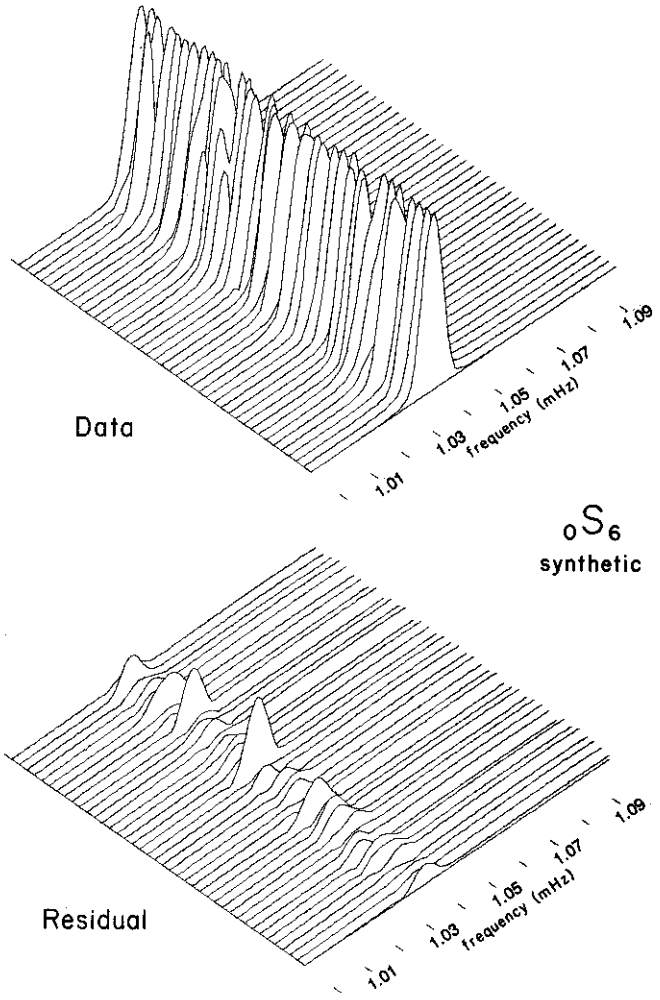

Fig. 5. Same as Figure 3*b* but for an experiment performed with synthetic data. Forty vertical component synthetic seismograms (top) were computed using model DW2 (degrees 1–8 structure as described in section 4), spectral fitting was performed and the estimated coefficients, listed in Table 5, were used to compute the residuals (bottom). The size of the residuals are similar to those in Figure 3*a*.

Evaluation of the quality of the coefficient estimates requires a careful analysis of misfit which we describe in section 3.2.

3.2. *Analysis of Misfit*

We consider equation (12) to be embedded in a noise process which can be represented by the error term $\boldsymbol{\varepsilon}(\omega)$:

$$\Delta \mathbf{s}(\omega) = \mathbf{A}(\omega)\delta\mathbf{c} + \boldsymbol{\varepsilon}(\omega)$$

Commonly, data errors are assumed to be Gaussian when all the statistical variability is thought to be due to measurement errors. In the present case the error term is complicated by the fact that **A** is itself a stochastic entity containing measured quantities as well as assumptions and approximations which might loosely be called signal-generated noise. Noise which is not generated by the signal results from a variety of sources, among which are aftershocks and other seismic events during the recording period, instrument malfunction, timing errors, atmospheric pressure variations, etc. If these sections of anomalous data are short enough, the data are zeroed or linearly interpolated. Records with more than a small percentage of bad data are rejected. Timing errors are sought and corrected during moment tensor retrieval. Though diminished, contamination of the spectrum due to these processes remains. Over narrow frequency bands, these processes are probably nearly frequency independent and produce what might be considered to be the ambient noise in each spectrum. If ambient noise were the only source of error, misfit would be at the ambient noise level. An examination of Figures 3 and 4 reveals that for even the best fit multiplets the residual is above the ambient noise level for the highest signal recordings. It is signal-generated noise which causes the standard error analysis to be inaccurate and is the main cause of error in the coefficient estimates.

Signal-generated noise derives generally from two sources: (1) measurement errors and approximations in **A** and (2) unspecified structure and multiplet-multiplet coupling. The first source of noise comprises errors in the radial eigenfunctions, in the estimates of the source mechanism and instrument responses, and in the numerical approximations used to construct the partial derivatives. Numerical approximations can be controlled to have a small effect. Nominal responses for both IDA instruments and GDSN instruments since 1980 appear, with a few exceptions, to

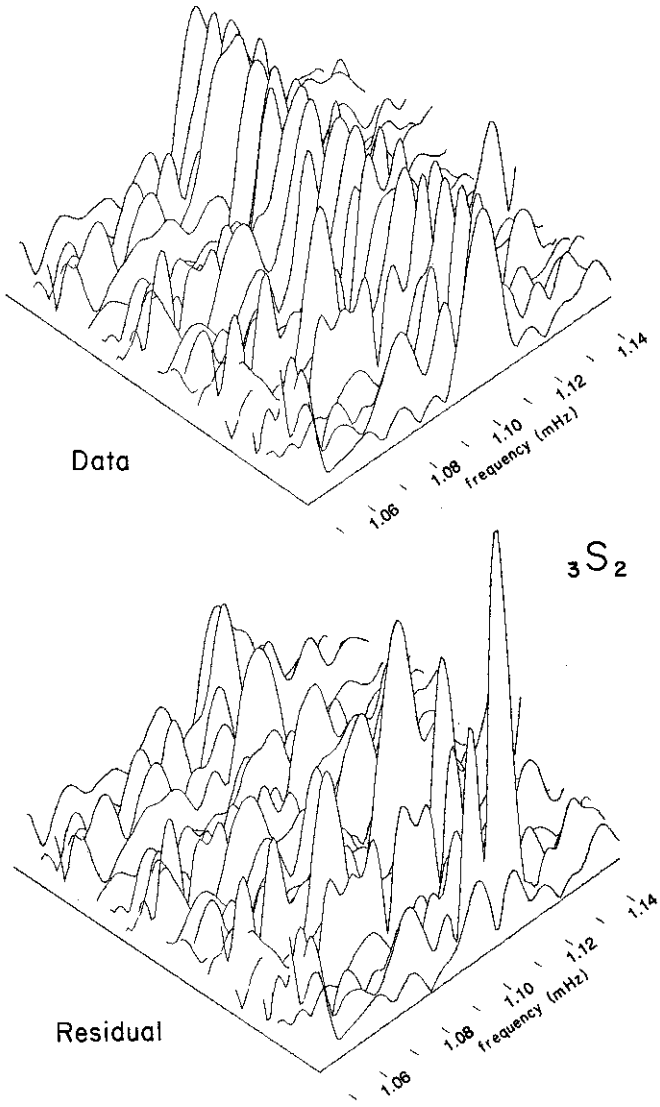

Fig. 6. Same as Figure 3*b* but for 22 of the recordings used for the anomalous multiplet $_3S_2$. Residuals for this and most of the other anomalous multiplets are, on average, above ambient noise levels.

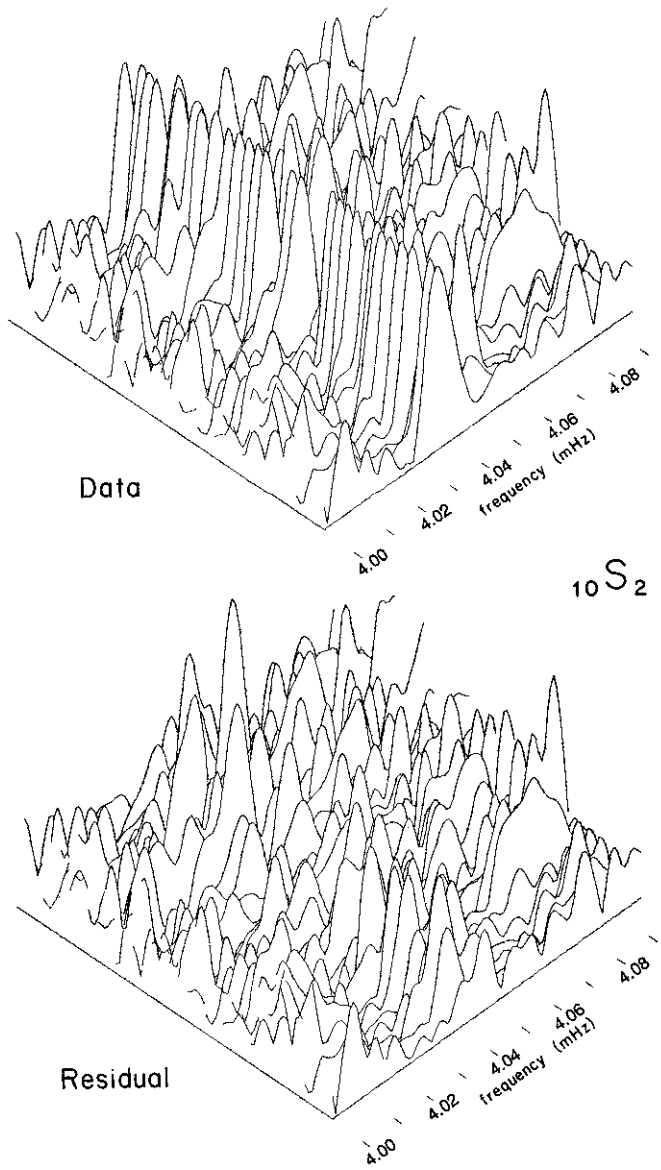

Fig. 7. Same as Figure 3*b* but for 45 of the recordings used for the anomalous multiplet $_{10}S_2$. The residual level for $_{10}S_2$ and other anomalous multiplets is frequently above ambient noise, believed to result from errors in the radial eigenfunctions.

be quite accurate. R. Woodward and G. Masters (unpublished manuscript, 1987) report the recalibration of the GDSN instruments prior to 1980 so that errors in instrument responses should not be a major problem when data from a number of events are included. Moment tensor estimates are used in the construction of the source vector $\mathbf{a}_k$ in equation (2) and are probably accurate to better than 10% of the moment for most events used here. At this level, errors in the moment tensor produce a relatively small effect on the coefficient estimates. Errors in the source time functions become more appreciable as frequency increases, producing relatively larger phase errors for higher-frequency multiplets. For example, an error of 10 s in the source time function produces a 4° phase error for $_0S_6$ but a 20° error for $_{13}S_2$. Higher frequency multiplets will be harder to fit, but it is expected that errors in the source time function are random, and general errors in the estimate of the source mechanism should not be a serious problem when data from a number of events are included. The radial eigenfunctions computed relative to a radial Earth model (1066A here) pervade the computations, going into the construction of σ_k, $\mathbf{a}_k$, and $_k\mathbf{G}_s(r)$. Their accuracy depends on the accuracy of the radial model at those depths where each mode is most sensitive. Errors in the radial eigenfunctions for the mantle sensitive modes are probably relatively small. (For example, the interaction coefficients computed relative to 1066A for the mantle modes with aspherical model Ms2 of section 4 differ by less than $0.1\,\mu$Hz from the coefficients computed relative to 1066B.) However, it is not unlikely that the radial eigenfunctions for the anomalous modes are in error since spherically averaged core structure is quite poorly constrained [*Stark et al.*, 1986]. A noteworthy example is the extreme dependence of the eigenfunctions of $_{10}S_2$ on the location of the inner core boundary (ICB). Although the location of the ICB in models 1066A and 1066B differ by less than 13 km, model 1066B mispredicts this mode to be trapped in the inner core.

The effect of unspecified higher-order structure is strongest on

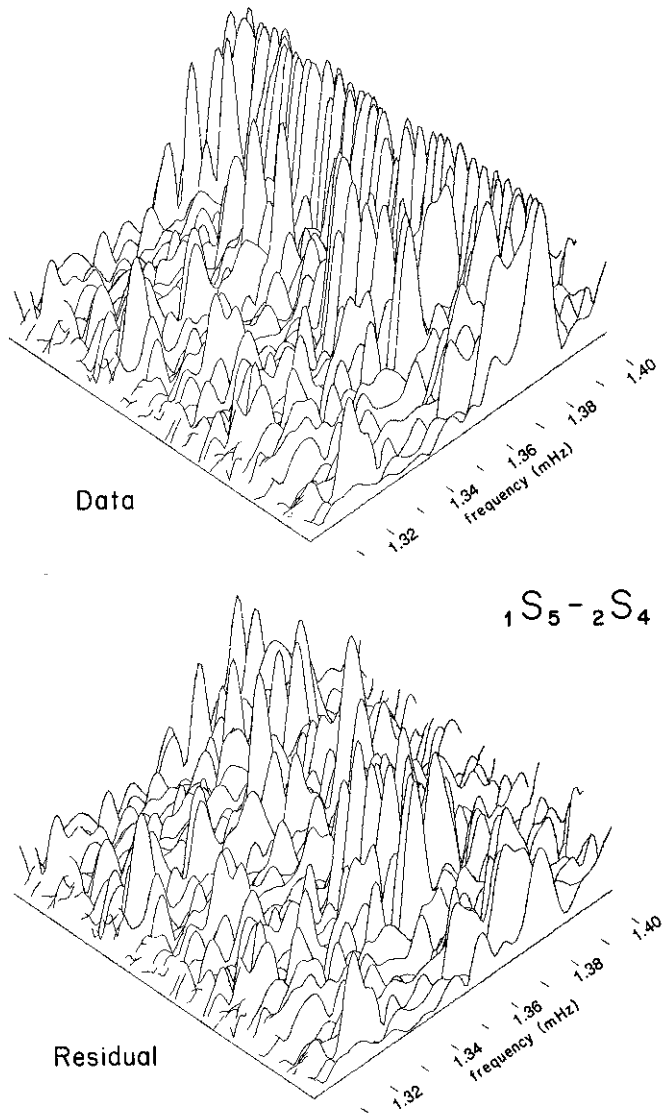

Fig. 8. Same as Figure 3*b* but for 55 of the recordings of the overlapping multiplets $_1S_5$ and $_2S_4$. The high residual level is indicative of coupling between these multiplets.

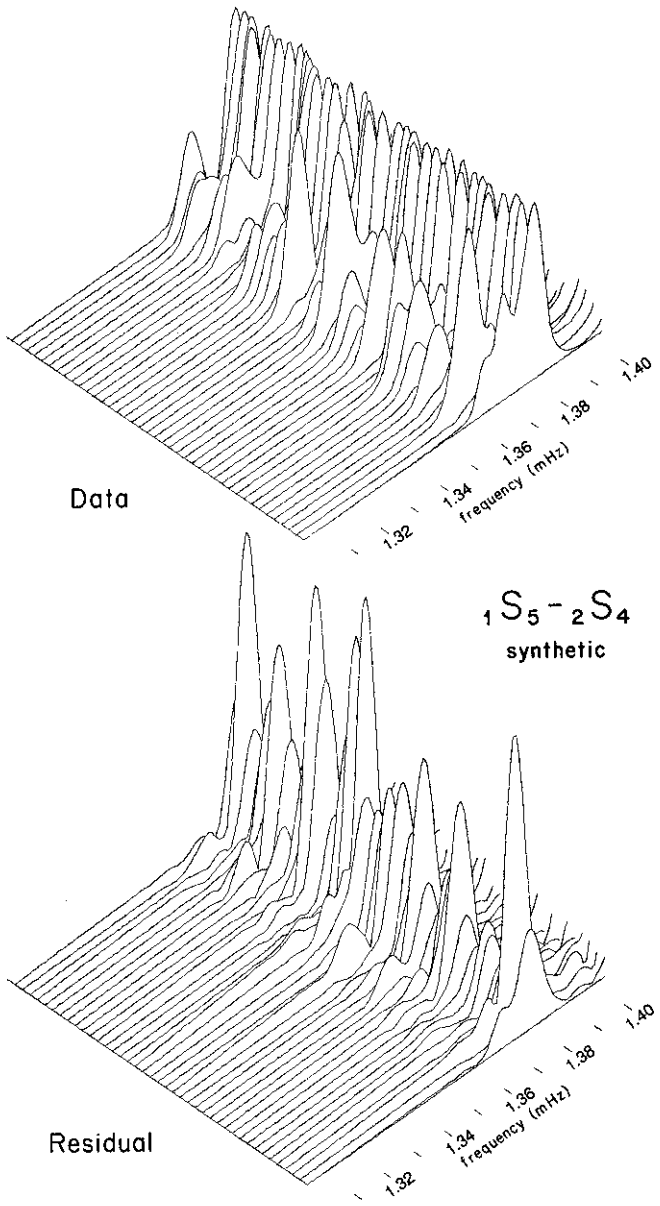

Fig. 9. Same as Figure 8 but for an experiment performed with synthetic data for ${}_1S_5$ and ${}_2S_4$ like that described in the caption for Figure 5 but with coupling between these modes. The large residuals indicate that ${}_1S_5$ and ${}_2S_4$ are coupling fairly strongly in the synthetic experiment but are larger than with real data (Figure 8). It is not unlikely that DW2 possesses more degree 1 and 3 structure (through which ${}_1S_5$ and ${}_2S_4$ couple) than the real data.

singlets with nearly degenerate cross-azimuthal coupling partners. Since the density of singlets within most multiplets is nonuniform, this contribution to the error term will be a strong function of frequency. A multiplet of harmonic degree ℓ is sensitive to spectral structure of degree and order up through 2ℓ. Since we estimate structure only up through degree 4, the biasing effects of higher-order structure potentially increase with increasing harmonic degree of the multiplet. (However, degree 2 multiplets such as ${}_3S_2$, ${}_{10}S_2$, and ${}_{13}S_2$ are fully specified.) Although we attempt to focus on isolated multiplets, weak coupling does contaminate some of the multiplets considered here, and the accuracy of spectral fitting depends critically on diagnosing when strong coupling is likely to occur. In section 3.2.2 we discuss the synthetic experiments which have been performed to determine the effect of weak coupling on the multiplets that we analyze. In summary, signal-generated errors are of extreme concern and are dependent on the multiplet considered, frequency, and source and receiver location. We should also mention that due to the smoothing characteristics of the taper in the frequency domain, they are also probably not independent.

In theory, a complete understanding of the statistical properties of each of the noise processes would lead to accurate estimates of the bias and variance of the coefficient estimates. Since we have no a priori estimate of these quantities, we are forced to try to bound their effect on the estimated coefficients with synthetic experiments. The relative importance of the noise processes differs among multiplets. For example, it is likely that the misfit to ${}_0S_6$ is dominated by ambient noise and higher-order structure, the misfit to fully specified anomalous modes (e.g., ${}_{13}S_2$, ${}_{10}S_2$, ${}_3S_2$) by errors in the radial eigenfunctions, and the misfit to overlapping multiplets (e.g., ${}_1S_5 - {}_2S_4$, ${}_1S_6 - {}_2S_5$) by multiplet-multiplet coupling. A first attempt at estimating the covariance matrix $\mathbf{C}_k$ of the interaction coefficients for multiplet k could be made with (14) used as an estimate of the inverse standard deviation for

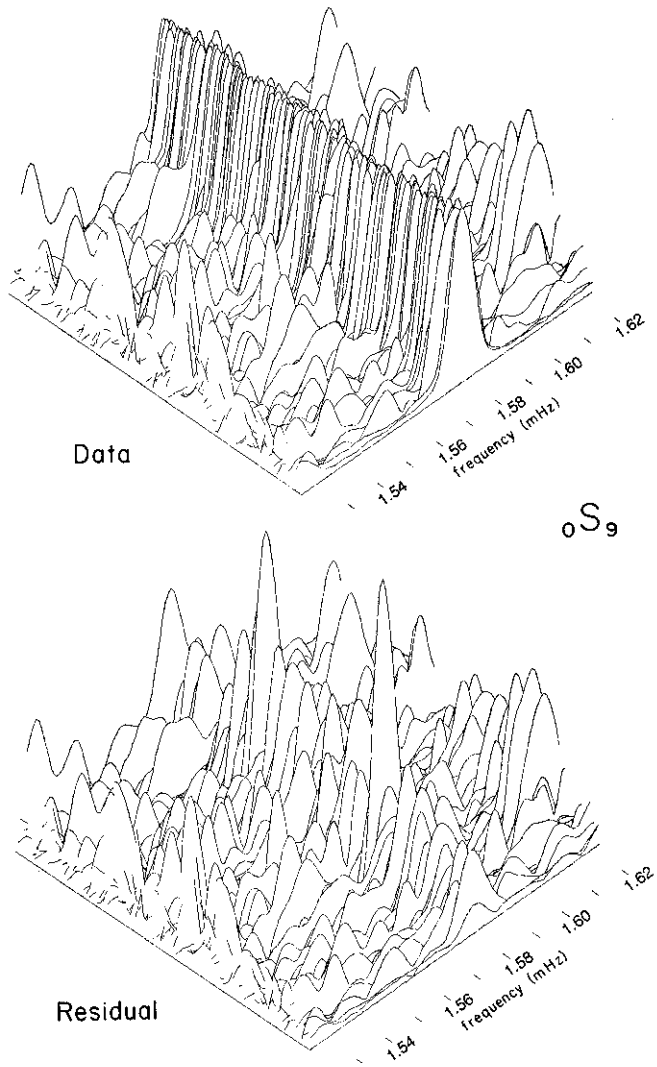

Fig. 10. Same as Figure 3*b* but for 108 of the recordings for ${}_0S_9$. Large residuals indicate Coriolis coupling to the nearby toroidal mode ${}_0T_{10}$ which appears, mostly on horizontal recordings, as peaks at the high-frequency end of the spectra.

TABLE 1. Event Specification

Event	Origin Time Year	Day	Time	Colatitude, deg	Longitude, deg	Depth, km	Number of Recordings IDA	SRO/ASRO	Total	Total Moment	Moment Tensor Elements M_{rr}	$M_{\theta\theta}$	$M_{\phi\phi}$	$M_{r\theta}$	$M_{r\phi}$	$M_{\theta\phi}$	Source Time,* s
1	1977	173	1208:33	112.88	184.10	65	7	21	28	14.10	−7.05	0.47	6.58	3.16	11.80	1.76	47
2	1977	231	0608:55	101.09	118.46	20	7	21	28	26.50	−26.48	23.57	2.91	0.20	−0.62	8.31	30
3	1979	346	0759:03	88.40	280.64	25	10	30	40	10.00	9.85	−1.15	−8.70	0.59	1.63	−3.17	50
4	1980	199	1942:23	102.53	165.92	33	8	13	21	7.00	6.55	−0.08	−6.47	1.80	0.28	2.01	17
5	1982	173	0418:40	97.34	126.04	450	13	10	23	1.40	−0.90	−0.08	0.98	0.59	0.17	0.66	5
6	1983	77	0905:50	94.88	153.58	70	14	0	14	8.75	7.99	−2.11	−5.87	−2.28	−0.99	4.36	10
7	1983	146	0300:00	49.54	139.10	24	11	0	11	6.22	5.99	−0.62	−5.37	0.79	−0.97	−2.13	5
8	1983	328	0530:34	97.48	128.16	179	14	13	27	1.77	1.47	−1.61	0.14	−0.47	0.65	0.30	3
9	1984	1	0903:39	56.32	136.89	368	13	0	13	0.65	0.29	0.11	−0.40	0.18	−0.44	−0.26	3
10	1984	38	2133:22	100.00	160.46	18	13	0	13	4.07	1.19	1.13	−2.32	−1.27	−2.88	1.59	3
11	1984	66	0217:21	60.62	138.93	457	13	0	13	1.59	−0.27	0.94	−0.67	0.53	−1.10	−0.59	3
12	1984	219	1201:52	90.08	122.51	242	14	12	26	1.09	−0.49	0.93	−0.43	0.39	0.62	0.16	7
13	1984	325	0815:16	84.84	125.12	202	12	12	24	1.74	−0.91	0.46	0.46	0.67	−1.31	−0.53	3
14	1985	62	2247:07	123.16	288.02	20	11	10	21	7.25	7.21	−0.19	−7.02	0.43	0.46	−1.21	22
15	1985	210	0754:44	53.81	70.89	99	12	11	23	1.87	1.76	−1.66	−0.10	−0.19	0.41	−0.62	15
16	1985	262	1317:57	71.48	257.73	20	12	0	12	10.30	5.15	−4.09	−1.06	8.03	−3.88	2.08	40
17	1986	127	2247:11	38.48	185.22	33	13	0	13	10.22	9.73	−8.68	−1.05	0.94	2.35	−3.54	25
18	1986	293	0646:10	118.10	183.57	33	12	0	12	5.74	2.59	−3.69	1.10	−1.42	2.00	−3.51	10
							209	153	362								

Moment tensor elements are in units of 10^{20} N m.
*Half-baseline width of the source time function.

record n. The coefficient variance estimates ($\boldsymbol{\sigma}_c^2 = \text{diag}\,\mathbf{C}$) are quickly shown to be too small by synthetic experiments with the inclusion of realistic amounts of signal-generated noise. In addition, simple changes in the experimental prescription (e.g., time series length and start time, row weighting scheme, SVD truncational level, etc.) frequently cause perturbations larger than these error estimates. Furthermore, since the way in which multiplets on the same dispersion branch sample the Earth changes smoothly along the branch, the coefficients should also vary smoothly along the branch within the errors estimated. This ensures consistency of the coefficients estimated from different multiplets. The along branch variability, although fairly smooth, is still too great to be encompassed by these simple error estimates. These reasons lead us to believe that estimated standard deviations have to be increased by a factor of 3–5 on average.

Although variances estimated in this way are too small, in most cases they probably reflect the relative sizes of the coefficient errors. Relative errors are dependent on the relative sensitivity of the data to the coefficients which are reflected by the elements of $\boldsymbol{\sigma}_c$. However, the estimated coefficient covariance matrix will not be related, in a straightforward manner, to the probability distribution of the estimated coefficients and therefore will not provide error estimates which are even relatively accurate across multi-

TABLE 2. Summary of the Fit to the Data

Multiplet	χ^2 Ratio* s=2,4	% χ^2 Reduction† s=2,4	Number of Recordings
${}_0S_2$	0.35	5	14
${}_0S_3$	0.15	20	32
${}_0S_4$	0.04	71	36
${}_0S_5$	0.10	78	73
${}_0S_6$	0.09	82	89
${}_0S_7$	0.08	87	108
${}_0S_7$–${}_2S_3$	0.13	83	108
${}_0S_8$	0.03	90	120
${}_0S_9$	0.06	79	146
${}_1S_3$–${}_3S_1$	0.11	33	44
${}_1S_4$	0.22	20	59
${}_1S_5$–${}_2S_4$	0.28	49	93
${}_1S_6$–${}_2S_5$	0.25	42	102
${}_1S_7$	0.16	75	60
${}_1S_8$	0.10	90	70
${}_1S_9$	0.20	76	37
${}_2S_3$	0.22	87	26
${}_2S_6$	0.16	74	82
${}_2S_8$–${}_4S_3$	0.28	65	143
${}_3S_2$	0.36	86	30
${}_5S_3$	0.11	73	36
${}_5S_4$	0.16	66	68
${}_5S_5$	0.13	63	93
${}_5S_6$	0.10	71	117
${}_5S_7$	0.16	76	75
${}_5S_8$	0.31	57	56
${}_6S_3$–${}_3S_8$	0.25	74	100
${}_8S_5$	0.22	86	60
${}_9S_3$	0.44	84	54
${}_{10}S_2$	0.31	91	52
${}_{11}S_4$	0.22	89	68
${}_{11}S_5$	0.10	92	83
${}_{13}S_2$	0.22	92	82
${}_{13}S_3$	0.34	89	68

*$\chi^2(\hat{\mathbf{c}})/\sum_{i,n}[s_n(\omega_i)/\sigma_n(\omega_i)]^2$, where $\sigma_n(\omega_i) = w_n^{-1}$ in (14) and $\chi^2(\hat{\mathbf{c}})$ is defined in (15).
†Relative to the RH model: $(1-\chi^2(\hat{\mathbf{c}})/\chi^2(\mathbf{0}))$.

TABLE 3. Degrees 2 and 4 Interaction Coefficient Estimates

	c_2^0	Re c_2^1	Im c_2^1	Re c_2^2	Im c_2^2	c_4^0	Re c_4^1	Im c_4^1	Re c_4^2	Im c_4^2	Re c_4^3	Im c_4^3	Re c_4^4	Im c_4^4
${}_0S_3$	0.80	−0.40	0.10	0.50	0.90	0.10	−0.20	−0.20	0.50	1.00	0.90	1.70	1.90	1.00
${}_0S_4$	1.50	0.40	0.10	−0.90	1.20	−0.20	0.10	−0.10	0.10	−0.30	0.50	−0.40	−1.50	0.50
${}_0S_5$	2.00	0.50	0.30	−1.30	1.60	0.20	−0.20	0.00	0.20	−0.30	0.00	0.30	0.50	−0.70
${}_0S_6$	2.30	0.50	0.20	−2.10	2.50	0.00	0.00	0.40	0.50	0.60	0.50	0.70	0.20	0.50
${}_0S_7$	1.70	0.90	0.10	−2.80	3.00	0.00	−0.30	−0.50	0.90	0.70	0.30	0.10	−0.20	−0.10
${}_0S_8$	1.30	1.10	0.10	−2.20	2.60	−1.00	0.60	0.50	0.20	0.40	0.70	1.00	−0.50	−1.30
${}_0S_9$	−0.80	1.40	−0.30	−2.40	3.70	0.10	−0.40	−0.20	0.10	0.50	1.40	0.70	0.20	0.20
${}_1S_3$	0.10	0.60	0.30	−1.30	2.20	0.60	0.20	−0.40	−0.70	−0.40	−0.90	0.00	−3.30	2.00
${}_1S_4$	0.60	0.30	0.60	−2.00	2.00	−0.50	−0.30	−0.40	0.90	0.40	−0.40	−0.40	0.70	−2.10
${}_1S_5$	2.10	0.40	0.80	−2.80	3.50	0.00	0.40	−1.80	5.00	1.00	−2.80	−3.30	−7.70	1.20
${}_1S_6$	0.80	0.10	−0.30	−6.10	3.70	1.00	0.20	0.70	1.50	−1.20	−1.40	0.40	0.80	2.90
${}_1S_7$	4.20	0.30	1.00	−4.30	1.90	−1.00	0.10	0.20	1.70	0.60	0.40	0.60	−0.50	−3.00
${}_1S_8$	5.30	0.70	1.10	−5.70	3.10	−1.00	0.90	0.60	1.90	−0.10	−0.20	1.30	−0.50	−0.50
${}_1S_9$	6.50	0.80	1.40	−7.00	4.10	−0.90	0.80	1.50	1.80	2.70	0.60	1.50	−1.50	1.50
${}_2S_3$	9.00	1.30	0.70	−3.50	2.60	1.00	0.90	0.40	0.20	0.20	0.70	0.20	0.20	0.50
${}_2S_4$	0.90	1.60	1.00	−3.40	2.80	−1.60	−0.70	0.50	2.30	−0.90	−0.60	0.60	−1.30	0.20
${}_2S_5$	0.70	2.60	2.10	−0.60	4.80	−0.20	1.50	1.00	−0.20	0.70	1.50	1.10	1.90	−1.00
${}_2S_6$	−2.00	3.10	1.60	1.60	5.10	0.80	−0.20	−0.10	0.90	−1.60	1.10	0.50	0.40	−1.80
${}_2S_8$	−4.80	4.10	2.10	0.40	9.50	1.40	0.60	−1.60	−1.60	0.20	1.50	0.90	−1.00	−2.50
${}_3S_1$	0.70	0.00	−0.10	0.00	1.30	—	—	—	—	—	—	—	—	—
${}_3S_2$	16.50	1.10	0.10	−2.30	5.70	5.10	1.50	2.50	−4.50	4.80	0.60	−0.40	−1.80	−2.00
${}_3S_8$	0.70	3.70	1.10	−4.60	11.50	−3.30	1.80	0.00	0.30	0.20	1.60	−1.30	−1.50	−1.00
${}_4S_3$	0.10	0.40	2.00	−1.60	1.50	1.50	1.30	−1.50	−2.40	0.60	1.80	0.40	1.70	0.50
${}_5S_3$	−0.50	−0.40	0.90	−5.40	5.30	−1.50	−1.40	0.00	−2.00	0.80	1.10	1.20	−2.10	0.40
${}_5S_4$	−0.30	0.50	1.90	0.50	5.20	1.90	1.10	−1.20	2.00	−0.40	0.50	−1.60	2.20	−0.70
${}_5S_5$	1.60	0.20	1.00	−0.20	2.90	0.60	0.80	−2.10	0.50	−1.80	−1.60	−0.10	1.70	−1.50
${}_5S_6$	2.60	0.30	1.70	−1.60	3.80	−0.10	1.00	−1.60	0.50	−0.90	−0.90	0.00	0.50	−0.50
${}_5S_7$	2.50	0.10	2.40	−2.60	3.00	0.20	0.70	−0.70	0.50	−0.30	−2.50	1.60	−0.50	−1.20
${}_5S_8$	4.70	−0.80	0.70	−3.00	5.30	0.60	−0.10	−1.90	1.20	−2.30	0.20	1.70	1.10	−1.80
${}_6S_3$	15.70	0.00	4.20	−1.80	4.00	6.70	−0.10	−2.50	−1.10	1.80	−2.70	−0.30	−0.50	0.40
${}_8S_5$	16.30	0.60	−0.20	−1.10	4.00	−2.50	−0.10	0.70	1.80	−1.50	−1.10	1.80	−1.30	−2.60
${}_9S_3$	16.50	−0.30	1.80	4.50	3.20	2.90	−1.00	−1.80	−7.00	−1.30	0.80	−2.00	0.30	−0.10
${}_{10}S_2$	21.50	−2.50	−1.90	−2.20	5.60	−1.60	0.80	0.50	−3.30	−4.80	1.90	3.80	−1.00	−0.10
${}_{11}S_4$	15.30	−1.00	3.30	−2.40	6.20	1.90	3.50	3.40	2.90	−1.80	4.60	−1.90	−3.10	−1.00
${}_{11}S_5$	10.20	−2.50	0.70	−4.70	4.20	0.60	0.20	−0.20	0.20	0.10	−4.00	−3.00	−2.00	3.00
${}_{13}S_2$	17.50	−0.60	0.50	−3.00	5.30	9.60	2.00	3.70	−0.70	−2.70	−2.20	1.80	1.90	−1.00
${}_{13}S_3$	17.10	2.20	−1.00	−8.50	2.80	0.30	2.60	4.00	1.20	−6.80	5.30	−0.70	1.30	−0.80

Estimates are in microhertz.

plets. This suggests that we should look to improve the covariance matrix estimates by rescaling them by some multiplicative factor α, $\mathbf{C}(\alpha)=\alpha^2\mathbf{C}$, which translates in a meaningful way across multiplets. In the present context, the coefficients are merely surrogates of the data, and we are interested in the distribution of the errors in the coefficients only insofar as they reflect our ability to model the data. This suggests that the errors should be rescaled relative to some notion of misfit to the data. Let $\hat{\mathbf{c}}$ be the estimated coefficient vector for a given multiplet and define misfit to the data in the usual chi-square sense:

$$\chi^2(\hat{\mathbf{c}}) = \sum_{i,n} [\Delta s_n(\omega_i)/\sigma_n(\omega_i)]^2 \tag{15}$$

where $\sigma_n(\omega_i)=w_n^{-1}$ from (14). We find that for most multiplets the variation in the coefficients found in the synthetic experiments can be encompassed by that perturbation to $\hat{\mathbf{c}}$ which changes χ^2 by about 20%. Thus we find α for each multiplet such that

$$\chi^2(\hat{\mathbf{c}}+\alpha\boldsymbol{\sigma}_c) = 1.2\,\chi^2(\hat{\mathbf{c}})$$

For example, for ${}_0S_6$, $\alpha=3.8$, which is within the 3–5 range prescribed by the synthetic experiments. For multiplets believed to be coupled, we use 40% change in χ^2 as the relevant significance level. Errors calculated in this way are listed in Table 4. In the following, we report synthetic experiments which show that these error estimates appear to be realistic. We must emphasize that these "errors" merely represent our confidence in the estimated coefficients. As shown in section 3.2.2, the estimator that we use for coupled modes is not unbiased, and the error estimates that we present are not to be interpreted as standard deviations of a Gaussian distribution. The solution to the problem of bias caused by multiplet-multiplet coupling is to generalize the current technique to encompass coupled modes. This is theoretically straightforward and is described by *Ritzwoller* [1987]. The application of this technique will be given in the second part of this paper.

3.2.1. *Uncoupled multiplets.* Although the size of $\boldsymbol{\varepsilon}(\omega)$ is potentially quite large, many multiplets are very well fit with the degrees 2 and 4 coefficients alone. Fits to the data are summarized in terms of chi-square ratios and chi-square reductions in Table 2. We tabulate these statistics for perusal by the reader, although they are not very useful indicators of how well the data are fit since a few extremely well fit or noisy recordings can dominate the statistic. Thus one should not infer from the fact that the χ^2 ratio for ${}_0S_9$ is lower than for ${}_0S_6$, that ${}_0S_9$ is fit better than ${}_0S_6$. In fact, it is not, as Figures 3*b* and 10 show. The χ^2 ratio is lower since the signal level is higher for ${}_0S_9$ than for ${}_0S_6$. For this reason we plot the residuals for a number of multiplets in Figures 3–10. Figures 3 and 4 display amplitude spectra of the data and residuals for the isolated low-frequency multiplets ${}_0S_6$ and ${}_1S_8$, respectively. In each plot, data amplitude spectra (top) are plotted so that peak

TABLE 4. Error Estimates

	c_2^0	Re c_2^1	Im c_2^1	Re c_2^2	Im c_2^2	c_4^0	Re c_4^1	Im c_4^1	Re c_4^2	Im c_4^2	Re c_4^3	Im c_4^3	Re c_4^4	Im c_4^4
${}_0S_3$	0.60	0.80	0.60	2.00	1.60	1.10	1.10	1.10	2.30	1.80	3.40	2.90	3.00	4.20
${}_0S_4$	0.50	0.30	0.50	0.60	0.90	0.50	0.40	0.50	0.60	0.60	0.90	0.80	1.70	1.50
${}_0S_5$	0.60	0.30	0.50	0.70	0.50	0.60	0.40	0.60	0.60	0.40	0.60	0.50	0.80	0.80
${}_0S_6$	0.60	0.30	0.40	0.60	0.50	0.60	0.30	0.50	0.40	0.40	0.50	0.50	0.50	0.70
${}_0S_7$	0.90	0.40	0.50	0.70	0.90	0.80	0.50	0.60	0.50	0.60	0.60	0.60	0.90	0.80
${}_0S_8$	0.60	0.20	0.20	0.20	0.60	0.40	0.10	0.20	0.20	0.30	0.20	0.20	0.40	0.30
${}_0S_9$	0.90	0.30	0.50	0.60	1.00	0.60	0.40	0.60	0.50	0.50	0.50	0.40	0.70	0.80
${}_1S_3$	0.70	0.70	0.70	1.70	1.80	1.00	1.00	1.10	1.60	1.60	2.50	2.30	3.50	3.20
${}_1S_4$	0.70	0.50	0.50	1.00	1.20	0.70	0.60	0.60	0.90	1.00	1.60	1.30	2.50	2.40
${}_1S_5$	1.40	0.90	0.80	1.70	1.30	1.40	1.10	1.20	1.70	1.60	1.90	1.60	6.00	3.30
${}_1S_6$	2.20	1.50	2.40	2.70	1.70	2.40	1.70	2.60	2.20	2.20	2.80	2.70	3.80	3.20
${}_1S_7$	1.40	0.60	1.00	1.60	1.00	1.30	0.80	1.10	1.30	1.00	1.40	1.00	1.80	1.60
${}_1S_8$	0.80	0.30	0.50	0.80	0.60	0.80	0.50	0.70	0.60	0.60	0.70	0.60	0.90	0.80
${}_1S_9$	3.60	0.70	1.60	3.90	2.50	2.20	1.00	1.80	2.10	1.50	1.50	1.70	2.60	2.50
${}_2S_3$	0.90	0.70	0.60	0.80	0.70	1.00	0.80	1.00	1.30	1.20	1.20	1.40	1.10	1.10
${}_2S_4$	1.10	0.60	0.70	0.90	0.90	1.20	0.70	0.80	0.80	0.70	1.10	0.90	0.80	0.90
${}_2S_5$	1.60	0.80	1.10	1.50	1.40	1.10	0.80	0.90	0.90	0.80	1.00	1.10	1.10	1.40
${}_2S_6$	1.30	0.60	1.10	1.30	1.30	1.20	0.70	1.10	1.00	0.80	1.10	1.00	1.30	1.70
${}_2S_8$	2.00	0.60	1.00	2.10	1.20	1.40	0.70	1.10	1.40	0.90	1.10	1.00	1.50	1.50
${}_3S_1$	0.70	0.30	0.30	0.40	0.40	—	—	—	—	—	—	—	—	—
${}_3S_2$	1.60	1.90	1.20	2.40	2.00	1.50	2.70	1.70	2.30	1.90	0.90	1.30	1.10	1.20
${}_3S_8$	1.50	0.80	1.10	1.00	1.50	1.30	0.80	1.00	1.10	1.00	1.10	1.00	1.00	1.30
${}_4S_3$	1.50	0.80	1.00	1.70	1.40	1.60	1.50	1.40	1.60	1.80	1.60	1.30	1.50	1.50
${}_5S_3$	1.20	0.70	1.10	1.30	0.80	1.40	1.30	1.40	1.30	1.20	1.50	1.10	1.30	1.20
${}_5S_4$	1.10	0.60	1.00	1.10	1.00	1.30	0.90	1.10	1.40	1.10	1.40	1.50	1.40	1.50
${}_5S_5$	1.10	0.50	0.70	1.10	1.00	1.10	0.70	0.80	1.00	0.90	0.90	1.10	1.20	1.10
${}_5S_6$	1.00	0.50	0.70	1.10	0.70	0.90	0.70	0.80	0.90	0.70	0.90	1.10	1.00	1.10
${}_5S_7$	1.30	0.50	0.70	1.70	1.00	1.00	0.60	0.70	0.90	0.70	0.70	0.80	0.90	1.10
${}_5S_8$	4.40	1.30	1.70	3.70	4.00	3.30	1.60	1.80	2.30	2.70	2.10	2.60	3.10	3.60
${}_6S_3$	1.10	0.90	1.00	1.30	1.20	1.50	1.30	1.30	2.00	1.70	2.60	1.70	1.40	1.20
${}_8S_5$	1.60	1.30	1.10	1.50	1.80	1.70	1.80	1.80	2.90	2.50	2.20	2.00	1.90	1.60
${}_9S_3$	2.40	2.20	2.50	3.10	3.10	1.90	3.20	2.20	4.20	4.40	3.80	4.40	1.50	1.80
${}_{10}S_2$	2.20	1.70	1.70	1.90	1.10	0.80	0.80	0.80	1.60	1.00	1.90	2.00	0.40	0.50
${}_{11}S_4$	1.50	0.80	0.60	1.30	1.10	1.00	1.10	1.00	2.40	2.00	1.90	1.90	1.40	1.10
${}_{11}S_5$	1.50	0.90	1.00	1.00	1.30	1.60	1.10	1.30	2.00	1.50	2.00	3.10	2.20	1.60
${}_{13}S_2$	1.80	1.00	0.90	1.40	1.00	0.50	0.90	0.60	1.30	0.90	0.90	0.90	0.40	0.40
${}_{13}S_3$	1.70	1.20	1.00	1.50	1.10	1.30	1.40	1.00	1.90	1.80	1.50	2.00	1.00	0.90

Estimates are in microhertz.

heights are normalized and are compared with those of the residuals (bottom). The residual spectrum is the amplitude spectrum of the difference between the data and the synthetic seismogram computed with the degree 2 and 4 coefficients tabulated in Table 3. The residuals plotted in this way accentuate both amplitude and phase differences between the data and synthetic spectra. Figures 3*a* and 4*a* show the data and residuals for a few high signal-to-noise recordings. Most of the data set is displayed in Figures 3*b* and 4*b*. On average, the amplitude and phase spectra for these and most other isolated, low-frequency multiplets are fit at approximately the ambient noise level. The source of the residual is therefore difficult to identify but is probably small enough not to cause serious biasing. However, the residual for a few of the the high signal-to-noise recordings shown in Figures 3*a* and 4*a* is above the ambient noise level. Figure 5 contains the data and residual plots for a synthetic experiment which shows that realistic higher-order structure (degrees 6 and 8 here) could produce residuals at this level. The amplitude of the bias caused by higher-order structure is a function of the magnitude of the higher-order coefficients and the correlation between the columns of the partial derivative matrix associated with the specified and unspecified coefficients. Synthetic experiments with reasonable amounts of higher-order structure indicate that bias from this source should be small, of the order of 0.1–0.2 μHz (see Table 5). Furthermore, regressions run with the inclusion of higher-order structure do not produce perturbations in lower order coefficients larger than the errors listed in Table 4.

Not all very low frequency multiplets are as well fit as ${}_0S_6$ and ${}_1S_8$. As Figure 6 shows, signal level is low and misfit is high for the anomalous mode ${}_3S_2$. The difficulty in fitting the data is probably due to errors in the radial eigenfunctions for this mode. Although it appears clear that ${}_3S_2$ is anomalously split, inferences from poorly fit modes such as this must be made only with extreme caution, and it is not unlikely that the errors listed in Table 4 are underestimated for this mode.

Conditions change at higher frequencies where signal-to-noise levels for the targeted multiplets worsen, errors in the source time functions become more significant, multiplets are more likely to overlap and potentially couple, and errors in the radial eigenfunctions are expected for the anomalous multiplets. Nevertheless, many multiplets are relatively well fit. Figure 7 shows the data and residuals for 45 recordings of the isolated anomalous multiplet ${}_{10}S_2$. The regression here is fully specified since ${}_{10}S_2$ is sensitive only to degrees 2 and 4 structure, but the sensitivity of ${}_{10}S_2$ to the poorly constrained region near the ICB implies that it is not unlikely that the radial eigenfunctions are less reliable than for the mantle sensitive multiplets. In fact, the fit to all the anomalous modes is not as good as might be expected from experience with

TABLE 5. Synthetic Experiment to Determine The Effect of Coupling and Higher-Order Structure on the Coefficient Estimates

	c_2^0 (μHz)		Re c_2^1 (μHz)		Im c_2^1 (μHz)		Re c_2^2 (μHz)		Im c_2^2 (μHz)	
	Input	Observed	Input	Observed	Input	Observed	Input	Observed	Input	Observed
${}_0S_6$	1.28	1.24	0.47	0.43	0.24	0.27	−2.00	−1.80	0.64	0.60
${}_0S_8$	1.52	0.72	0.55	−0.12	0.02	−0.08	−2.45	−2.47	0.45	0.14
${}_0S_9$	1.37	−1.34	0.56	0.78	−0.30	−0.63	−2.20	−1.36	0.29	1.55
${}_1S_5$	0.35	1.40	1.01	0.70	−0.27	1.20	−1.10	−1.04	1.64	2.16
${}_1S_6$	1.12	−2.44	0.76	1.77	0.00	−4.34	−2.37	−3.91	0.96	1.26
${}_2S_4$	1.51	2.20	0.76	1.30	0.37	0.00	−1.99	−2.45	1.22	1.21
${}_2S_5$	0.56	1.37	1.16	−0.26	−0.15	−0.44	−0.44	0.65	2.02	0.48

Only degree 2 coefficients are tabulated.

mantle modes. Apparently, the spherical Earth model is inaccurate in the core in some way. Difficulties in fitting the degenerate frequencies of the anomalous multiplets also point to this conclusion (G. Masters and F. Gilbert, unpublished manuscript, 1987). We discuss this further in section 4.3. Since the way in which current core models are inaccurate is not known, the effect on the coefficient estimates cannot be determined. To try to compensate for this, we use a 40% change in χ^2 as the significance level for the anomalous multiplets, but confidence in the coefficient estimates for these modes awaits more accurate spherical models. Interpretation is further complicated when two or more multiplets overlap in frequency. Overlapping multiplets may be uncoupled if their Q values are appreciably different or if they sample the Earth in very different ways. An example of this is the pair ${}_{11}S_4 - {}_3S_{21}$ whose Q values differ by approximately a factor of 3. It is difficult to estimate the interaction coefficients for these two multiplets simultaneously since the optimum time series length for ${}_3S_{21}$ is much shorter than for ${}_{11}S_4$. However, the coupling between these multiplets is probably very weak and synthetic experiments show that the passive effect of ${}_3S_{21}$ on the estimation of the coefficients for ${}_{11}S_4$ is not great, probably less than 0.5 μHz for each coefficient. The fact that a contaminating multiplet shares the fitting band with ${}_{11}S_4$ explains why it, as well as ${}_{11}S_5$, ${}_{13}S_3$, and ${}_8S_5$, are not as well fit as the purely isolated multiplets ${}_{10}S_2$ and ${}_{13}S_2$.

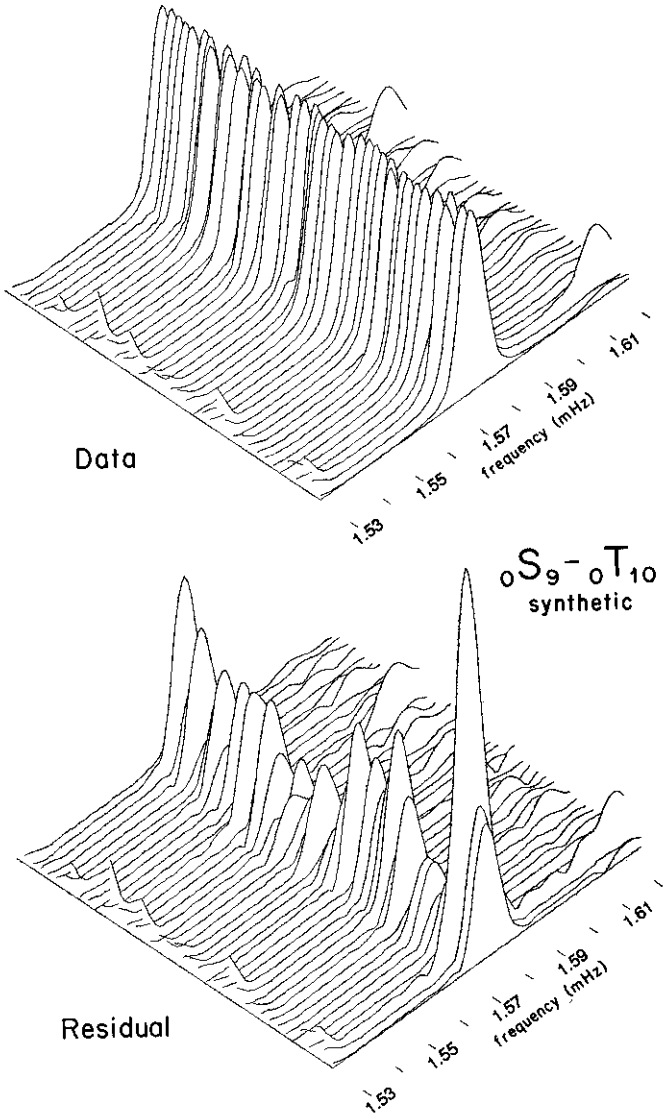

Fig. 11. Same as Figure 10, but for an experiment performed with synthetic data for ${}_0S_9$ like that described in the caption for Figure 5 but with Coriolis coupling between ${}_0S_9 - {}_0T_{10}$. The residual levels from the real data (Figure 10) and the synthetic data are qualitatively similar, indicating that the large residuals for ${}_0S_9$ likely result from Coriolis coupling to ${}_0T_{10}$.

3.2.2. *Weakly coupled multiplets.* We consider a number of multiplets which possess possible coupling partners: e.g., ${}_1S_3 - {}_3S_1$, ${}_1S_5 - {}_2S_4$, ${}_1S_6 - {}_2S_5$, ${}_2S_8 - {}_4S_3$, ${}_0S_8 - {}_0T_9$, ${}_0S_9 - {}_0T_{10}$, etc. With the exception of ${}_1S_3 - {}_3S_1$, residuals for each pair are generally greater than for isolated multiplets with approximately the same signal-to-noise level, implying that it is likely that the pairs are coupling. We discuss two examples here. First, the pairs ${}_1S_5 - {}_2S_4$ and ${}_1S_6 - {}_2S_5$ each overlap, and coupling could occur between the members of each pair through degrees 1 and 3 aspherical structure. However, ${}_1S_6$ and ${}_2S_5$, being closer in Q, should couple more efficiently than ${}_1S_5$ and ${}_2S_4$. In agreement with this expectation the residuals for ${}_1S_6 - {}_2S_5$ are appreciably larger than for ${}_1S_5 - {}_2S_4$. Figure 8 shows the data and residual plots for 55 of the recordings of ${}_1S_5 - {}_2S_4$. Table 5 presents the results of a synthetic experiment to determine the effect of coupling and higher-order structure on the coefficient estimates for these multiplets. Forty noise free synthetic seismograms computed with the inclusion of coupling between nearby neighbors were constructed using the upper mantle model M84A (degrees 1–8) and the lower mantle model LO2.56 (degrees 1–6) [*Woodhouse and Dziewonski*, 1984; *Dziewonski*, 1984] (model DW2 defined in section 4) and were then inverted only for the degrees 2 and 4 interaction coefficients. The errors in the coefficient estimates are at the 0.5–1.0 μHz level for ${}_1S_5 - {}_2S_4$ and the 1–2 μHz level for ${}_1S_6 - {}_2S_5$ and are reflected in the error estimates in Table 4. For comparison, Figure 9 shows the data and residuals for the synthetic seismograms for ${}_1S_5 - {}_2S_4$. The fact that the synthetic data are fit more poorly than the real data indicates that DW2 predicts greater coupling for these multiplets through degrees 1

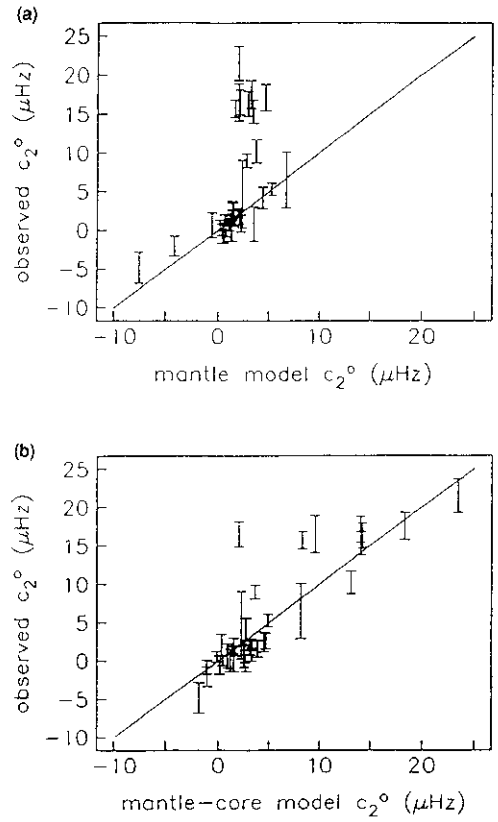

Fig. 12. Observed c_2^0 coefficients plotted versus predicted values. (*a*) Reference model is Ms2. (*b*) Reference model is Ms2 together with aspherical structure on the CMB, ICB, and isotropic heterogeneity in the volume of the inner core.

and 3 structure than exists. The results of this synthetic experiment should therefore be considered conservative. Second, we consider possible Coriolis coupling between low harmonic degree spheroidal and toroidal modes. Coriolis coupling between spheroidal and toroidal multiplets which differ in harmonic degree by 1 should increase as the spheroidal-toroidal branch crossing is approached at ${}_0S_{11}-{}_0T_{12}$. This is what is observed, and in particular, the residuals for ${}_0S_8$ are lower than those for ${}_0S_9$ which are shown in Figure 10. Figure 11 displays the synthetic data and residuals for the coupled pair ${}_0S_9-{}_0T_{10}$ which are in qualitative agreement with the results with the real data. The errors in the estimated coefficients for ${}_0S_8$ and ${}_0S_9$ in the synthetic experiment are also contained in Table 5 and are approximately 0.5 and 1.0 μHz, respectively. These are probably realistic errors and are reflected in the values tabulated in Table 4. Coriolis coupling and along-branch coupling for fundamental spheroidal modes above harmonic degree 9 become strong enough to vitiate completely the results with the current technique. We therefore exclude them from this analysis. The estimation of accurate interaction coefficients for any of these higher-order multiplets requires the extension of the technique to include multiplet-multiplet coupling. We are optimistic about the application of the generalized technique described by *Ritzwoller* [1987] to these high signal multiplets.

In conclusion, there are many sources of error which affect and could potentially bias the coefficient estimates found in Table 3. The relative importance of these sources of error varies among multiplets, but in most cases the error estimates listed in Table 4 appear to encompass the expected perturbation in the estimated coefficients.

4. Interpretation and Inference

The 38 multiplets for which interaction coefficients have been estimated and listed in Table 3 partition naturally into two groups: the 10 anomalously split multiplets (${}_2S_3$, ${}_3S_2$, ${}_6S_3$, ${}_8S_5$, ${}_9S_3$, ${}_{10}S_2$, ${}_{11}S_4$, ${}_{11}S_5$, ${}_{13}S_2$, ${}_{13}S_3$) and the remaining normally split, mantle sensitive modes. These groups are distinguished by the size of their c_2^0 coefficients which are very large for the anomalous modes. Figure 12*a* shows the observed c_2^0 coefficients for all 38 multiplets compared with the c_2^0 coefficients computed for the aspherical model Ms2 described below. The cloud of observations above the diagonal line belongs to the anomalous modes and cannot be fit with mantle structure alone. *Ritzwoller et al.* [1986] argued that the source of anomalous splitting, in all probability, lies in the core. In this section we first discuss the inversion of the

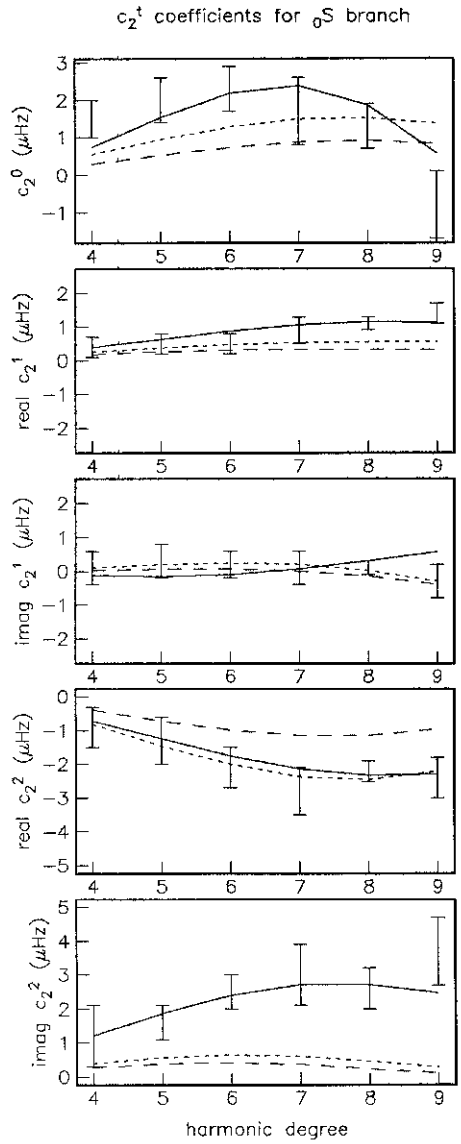

Fig. 13. Estimated degree 2 coefficients and error estimates plotted versus harmonic degree along the fundamental mode branch. The dashed and dotted curves represent the predicted values from DW1 and DW2, respectively, and the solid curve represents the values from our model Ms2.

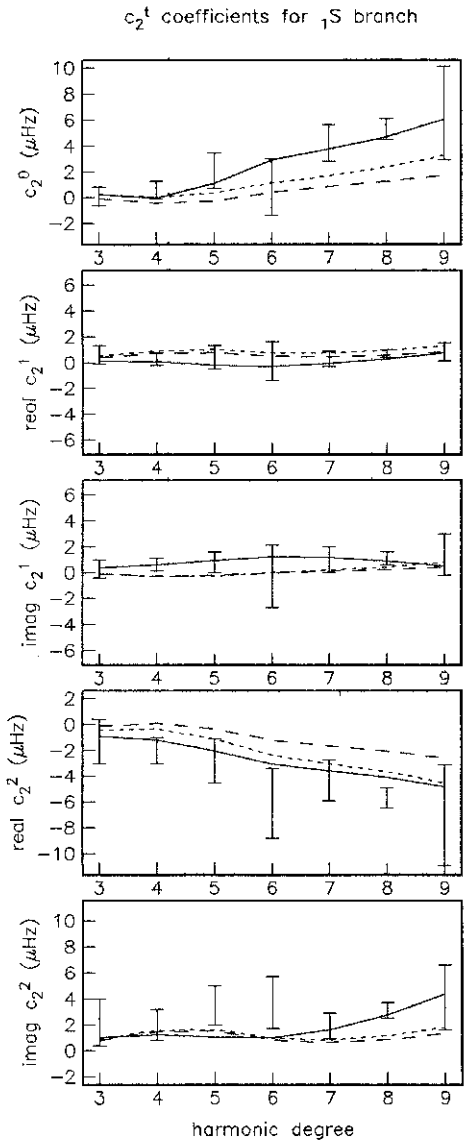

Fig. 14. The $_1S$ branch (same as Figure 13).

degree 2 interaction coefficients from the 28 mantle sensitive modes for mantle structure, comparing the retrieved model with the models M84A [*Woodhouse and Dziewonski*, 1984] and LO2.56 [*Dziewonski*, 1984]. Afterward, we briefly discuss anomalous splitting.

4.1. *Consistency of Estimated Interaction Coefficients With Existing Mantle Models*

The coefficients presented in Table 3 are insufficient, both in number and accuracy, to resolve uniquely the low-order aspherical structure of the mantle. Therefore we consider only models which are smooth functions of radius. The degree 4 coefficients are, on average, smaller than the associated errors in Table 4 so we confine attention to degree 2 structure alone. (More accurate estimation of degree 4 interaction coefficients will require more recordings per multiplet than are currently available.) For $_0S_2$ the lowest-frequency observed mode, the estimated degree 2 coefficients are very poorly constrained and are therefore not listed in Table 3. As argued in section 3, since the sensitivity to aspherical structure changes smoothly along a single dispersion branch, a smooth model will fit the interaction coefficients only if the coefficients vary smoothly along each branch. Figures 13–16 show the degree 2 coefficients and errors plotted along the $_0S$, $_1S$, $_2S$, and $_5S$ branches. Figure 17 represents the degree 2 coefficients determined from multiplet center frequency observations for the fundamental surface wave equivalent modes $_0S_{20}-{}_0S_{40}$ [*Smith et al.*, 1987]. Since these multiplets are all dominantly sensitive to structure in the mantle and, on average, the coefficients vary smoothly along each branch within the estimated errors, the coefficients should be able to be fit with a simple model of mantle structure. As will be discussed later, a few of these multiplets are also sensitive to core structure, especially in the top of the outer core. They will therefore also have to be treated further when hypotheses concerning the cause of anomalous splitting are considered.

As discussed in section 1, the comparison of the estimated coefficients with the coefficients predicted by existing models of aspherical structure is complicated by the fact that the computation of the c_s^l with (6) requires that the model be expressed as a

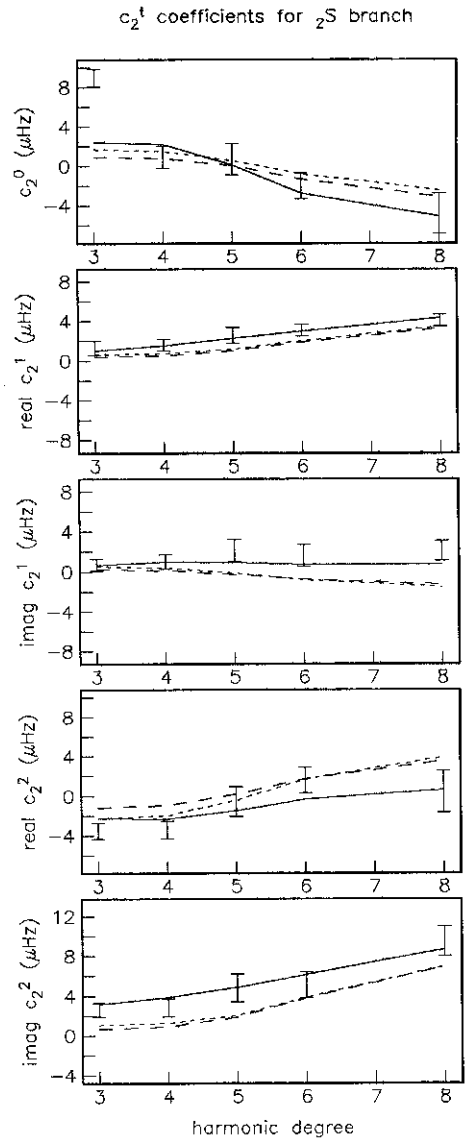

Fig. 15. The $_2S$ branch (same as Figure 13).

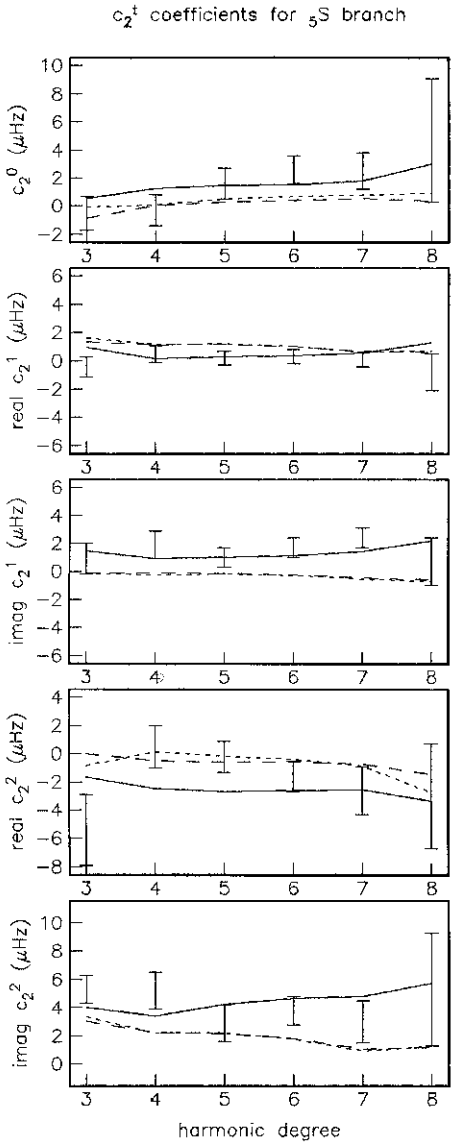

Fig. 16. The $_5S$ branch (same as Figure 13).

function of both κ and μ (or v_s and v_p), as well as ρ, rather than simply as v_s or v_p alone. The way in which simple functions in v_s or v_p should be translated into a form useful in low-frequency seismology is subject to debate. Experimental mineralogical evidence taken at upper mantle conditions suggests that the following relationships may be appropriate:

$$\frac{d \ln v_s}{d \ln \rho} = 2.5 \qquad \frac{d \ln v_s}{d \ln v_p} = 1.25 \tag{16}$$

(We call the model produced by M84A and LO2.56, using (16), DW1.) As described in section 1, the global relevance of these relationships is questionable, and there are those who advocate a scaling in which the constant in the right-hand equation in (16) is approximately doubled. We call this model DW2. Since the upper mantle model M84A is purely v_s, DW1 and DW2 differ only in the lower mantle where perturbations in v_s and ρ are twice as large for DW2 than for DW1.

The coefficients predicted by DW1 and DW2 are represented by the dashed and dotted curves in Figures 13–17, respectively. The fit to most of the coefficients along the $_0S$ and $_1S$ branches in Figures 13 and 14 is dominated by the lower mantle parts of DW1 and DW2. The improvement in fit to the estimated coefficients afforded by DW2 is confined to a few coefficients, deriving principally from the c_2^0 and real part c_2^2 coefficients along the $_0S$ and, to a lesser degree, the $_1S$ branches. The improvement in fit to these coefficients can as easily be accommodated by a CMB perturbation as a change in scaling. Except for these cases, DW1 and DW2 predict very similar coefficients. The misfit along the $_2S$ and $_5S$ branches in Figures 15 and 16 and to the higher-degree fundamental mode coefficients (Figure 17) is common to both models. It is encouraging to note that in nearly every case the predictions by DW1 and DW2 are of the right sign and trend along each branch.

Table 6 summarizes the fit to the coefficients from the mantle sensitive multiplets and from the surface wave multiplets with DW1 and DW2. Fit is represented by χ^2:

$$\chi^2 = \sum_k (c_k - c_k^p)^2 / \sigma_k^2$$

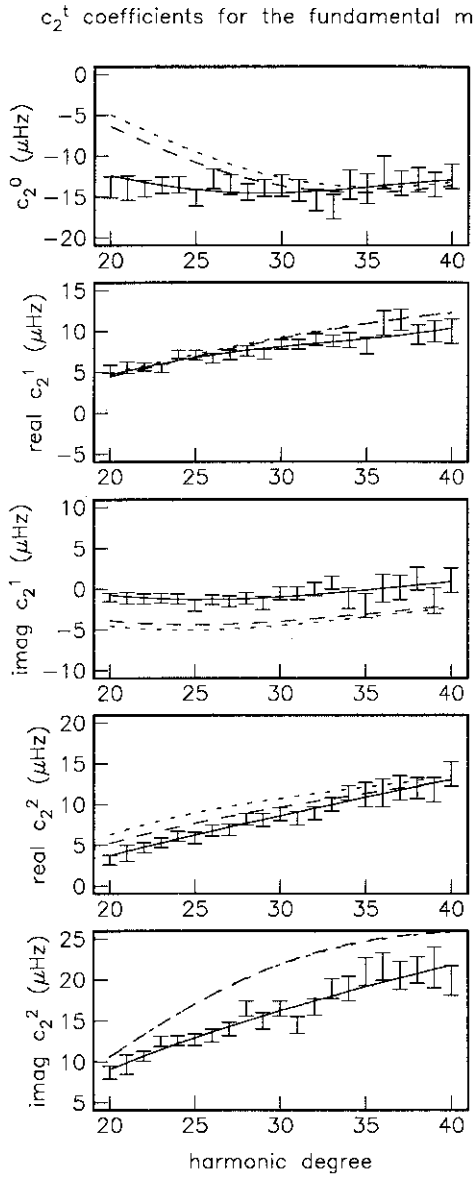

Fig. 17. Coefficients estimated from the center frequency measurements [*Smith et al.*, 1987] for $_0S_{20} - {}_0S_{40}$ (same as Figure 13).

TABLE 6. Misfit Statistics for Three Mantle Models

	140 Mantle Mode Coefficients		105 Fundamental Mode Coefficients		Total	
	χ^2	Variance Reduction, %	χ^2	Variance Reduction, %	χ^2	Variance Reduction, %
DW1*	469	52	831	89	1300	85
DW2†	328	66	1204	84	1532	82
Ms2‡	111	90	64	99	200	98

* LO2.56 and M84A with $v_s : v_p$ ratio equal to 1.25.
† LO2.56 and M84A with $v_s : v_p$ ratio equal to 2.50.
‡ Our model.

where c_k is the observed coefficient (found in Table 3), c_k^p is the coefficient predicted by the model, and σ_k is to coefficient error (found in Table 4) for multiplet k. (This statistic represents the misfit of a model to the interaction coefficients and should not be confused with $\chi^2(\hat{\mathbf{c}})$ in (15), which represents the size of the residual spectrum.) We seek models which, on average, predict interaction coefficients approximately 1σ from the observed coefficients. For an acceptable fit, $\chi^2 \approx K$, where K is the number of coefficients used. The total χ^2 of the $28 \times 5 = 140$ degree 2 coefficients for the mantle sensitive multiplets relative to DW1 is 469 and is 328 relative to DW2. Similarly, χ^2 of the $21 \times 5 = 105$ surface wave multiplets is 831 and 1204, respectively. Total variance reductions relative to the RH model (for which all coefficients are zero) are 85% for DW1 and 82% for DW2. The reduction in variance by these models is large; however, with either scaling relationship a lot of signal remains to be fit, and it seems worthwhile to consider constructing smooth models which do fit these data in detail.

4.2. *Mantle Models*

We first turn attention to aspherical structure in the mantle. As data we use the degree 2 interaction coefficients from the 28 low harmonic degree mantle sensitive multiplets (Table 3) and the coefficients from the 21 surface wave multiplets [*Smith et al.*, 1987]. We also require that models fit the geoid [*Lerch et al.*, 1985]. We follow *Gilbert et al.* [1973] and construct smooth models between seismic discontinuities by minimizing the sum of the Euclidean norm of the second radial derivative of $\delta \mathbf{m}_s^l(r)$ and the Euclidean norm of the boundary perturbations. This procedure is summarized in the appendix. The number and quality of data are insufficient to solve independently for all three functions of radius δv_s, δv_p, and $\delta \rho$. We use the scaling relationships in (16) to produce combined representers and present models only in relative shear velocity $\delta v_s / v_s$ for each order of degree 2 structure.

The simplest model of mantle structure would be smooth across the entire mantle, but we have been unable to produce a nonoscillatory smooth model which will fit all of the data. The reason lies in a competition between the surface wave coefficients and the geoid, apparently requiring oscillatory upper mantle structure at some azimuthal orders to resolve the conflict. We consider the mantle to comprise three layers: the lower mantle (3484–5700 km), the transition zone (5700–5950 km), and the uppermost mantle (5950–6360 km). We allow the constructed aspherical models to jump discontinuously at the boundaries around these regions irrespective of the existence of first-order discontinuities of the aspherical model at the layer interfaces. These jumps are introduced merely as a mathematical convenience and are not necessary attributes of models which fit the data. We are able to fit all the data with volumetric mantle structure alone, but the mantle is surrounded by two first-order discontinuities which potentially also possess aspherical perturbations. The Moho possesses a large degree 2 pattern due to variability in crustal thickness between continents and oceans. Whether long-wavelength aspherical boundary perturbations can exist on the CMB is currently under debate [*Gwinn et al.*, 1986; *Creager and Jordan*, 1986*b*; *Morelli and Dziewonski*, 1987]. Observational evidence for the existence of global first-order discontinuities at 400 and 670 km is subject to contention [*Silver et al.*, 1985] and spherically symmetric models exist covering both cases (e.g., model 1066A or model 1066B and PREM).

An unfortunate trade-off exists between aspherical boundary and volumetric perturbations. For example, *Masters et al.* [1982] described how the 21 surface wave coefficients alone could be fit with a wide variety of models, including a simple transition zone volumetric model or aspherical boundary perturbations on both sides of the transition zone. This ambiguity can only be resolved if either tight a priori bounds on the allowable boundary perturbations exist or if many different kinds of modes sample and thus constrain the region(s) of interest. Similar, though less extreme, ambiguities remain in the current study. A priori information on crustal structure is available in the form of tectonic regionalizations, although existing regionalizations differ substantially. *Woodhouse and Dziewonski* [1984] constructed a seismic crustal correction relative to preliminary reference earth model (PREM) from the regionalization of *Mauk* [1977]. Relative to the data in the current experiment, this correction is dominanted by a 6-km mantle bulge on the Moho under the Pacific Ocean (Figure 18*a*). which strongly imprints the data, making the surface wave multiplets and the geoid harder to fit especially for $\mathrm{Im}(Y_2^2)$ structure. We report here only models in which the Moho is unconstrained by a crustal correction, and due to the previously mentioned trade-offs (on top of the poor intrinsic resolution of the data set), uppermost mantle structure cannot be inferred unambiguously. Lowermost mantle structure is only weakly dependent on whether CMB perturbations are allowed in the inversion, and we report models in which the CMB is free as well. When the CMB is fixed, lowermost mantle structure is increased slightly in amplitude.

Much more disquieting is the strong dependence of middle mantle structure on the size of the aspherical perturbation allowed on the 400- and 670-km discontinuities. (To construct aspherical perturbations to these boundaries, we use 1066B as a radial reference model since it, unlike 1066A, possesses first-order discontinuities there. Since PREM has smaller jumps at 650 and 400 km than 1066B, aspherical models referenced to PREM would have to have larger perturbations on these boundaries to produce the same effect as those referenced to 1066B.) The nature of these discontinuities is not as well understood as the Moho or the CMB, but presumably these two features are at least in part associated

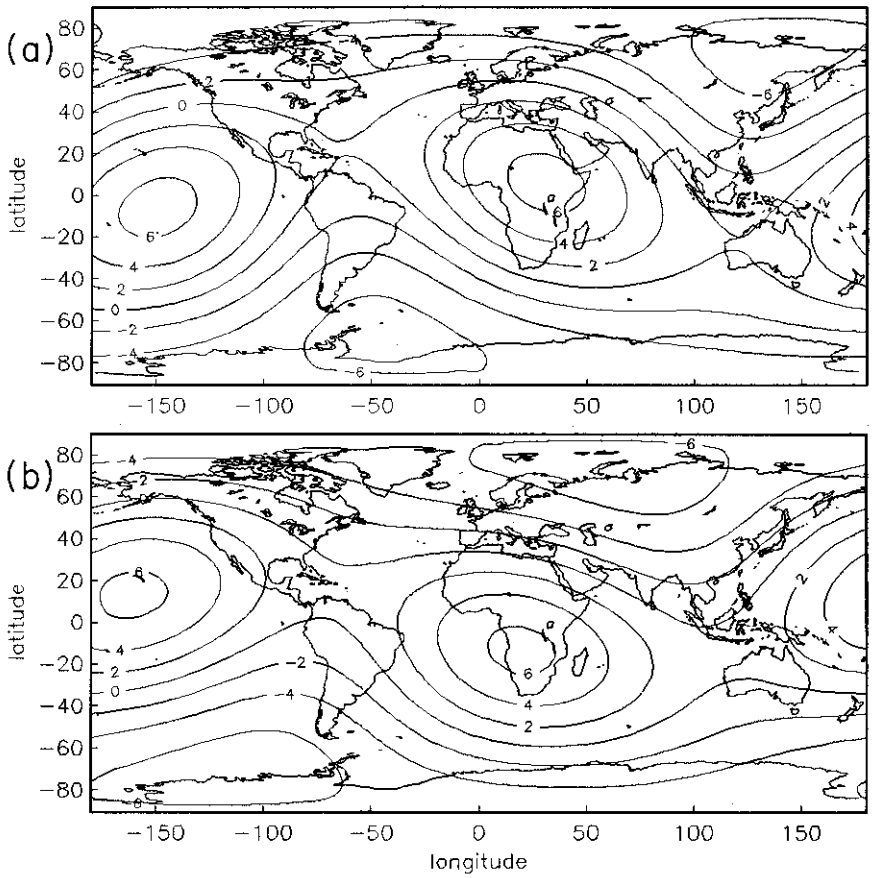

Fig. 18. (*a*) Comparison between the Moho perturbation we estimate and (*b*) that of the crustal correction of *Woodhouse and Dziewonski* [1984]. Contours are in kilometers.

with phase transformations; (olivine → spinel) at 400 km [*Ringwood*, 1975] and, more speculatively, (spinel → perovskite + magnesiowüstite) and (ilmenite → perovskite) at 670 km [*Liu*, 1979; *Yagi et al.*, 1979; *Ito and Yamada*, 1982]. Any perturbation which affects the local pressure or (probably more importantly) temperature regimes can produce lateral variations in the location of the phase changes. Figure 19 shows two models which fit the c_2^0 coefficients, one without structure on these boundaries (dashed line) and one with approximately 30 km on both boundaries (solid line). In fact, the model without the boundary perturbations fits the data quite a bit better, but unless structure of this magnitude can be safely ruled out on these discontinuities, we cannot even unambiguously infer the qualitative nature of mantle structure over large stretches of the middle mantle. (It should be pointed out that this problem is not unique to inversions with this data set but is probably common to other inversions with long-period surface wave data.)

Creager and Jordan [1986*a*] argue that the total aspherical perturbation to the 400- and 670-km discontinuities produced by slab penetration is probably less than 100 km. The degree 2 part of the slab component of the regionalization of *Okal* [1977], which contains a substantial slab contribution, is less than 5%. It is therefore unlikely that more than 5 km of perturbation to these discontinuities should arise due to slab penetration alone at degree 2. *Hager* [1984] argued that if slabs do not penetrate the 670-km boundary and pile up above it, then perhaps more than 60 km of deflection could occur and would be distributed over a wider area than if the slabs penetrated into the lower mantle. Whether this area would be greater than the 5° × 5° slab region in Okal's regionalization is debatable, but if these two mechanisms are the principal potential causes of boundary deflection in the middle mantle, then a 5–10 km maximum at degree 2 is probably reasonable. For this reason, since a 5-km perturbation to these boundaries does not substantially change the inferred volumetric structure, we report further only models without perturbations to the 400- and 670-km boundaries. To the extent that the reader finds this argument unsatisfying, inferences about middle mantle structure must be met with suspicion.

We call the smooth degree 2 model (constructed with a free Moho and CMB but with fixed 670- and 400-km discontinuities) Ms2 (for mantle, s=2). Ms2 is shown in Figure 20 (solid line) with DW1 (dashed line) plotted for comparison. The fit to the data is summarized in Table 6. The total χ^2 produced by Ms2 for the 140 degree 2 coefficients is 111, and the χ^2 for the 105 degree 2 surface wave coefficients is 64 for a total variance reduction of 98%.

The lower mantle part of Ms2 is qualitatively similar to DW1. Both are dominated at most depths by Y_2^0 and/or Y_2^2 heterogeneity, but the two models differ substantially in amplitude. The lower mantle part of both models is characterized by the concentration of structure near the boundaries (CMB and 670 km). Ms2 and DW1 are qualitatively very similar in the lowermost mantle and contour plots of the two models nearly overlie (Figure 21). Neither model shows much structure in the mid-lower mantle. Structure does differ considerably near the top of the lower mantle, however, with Ms2 being dominated by Y_2^0 and DW1 by a

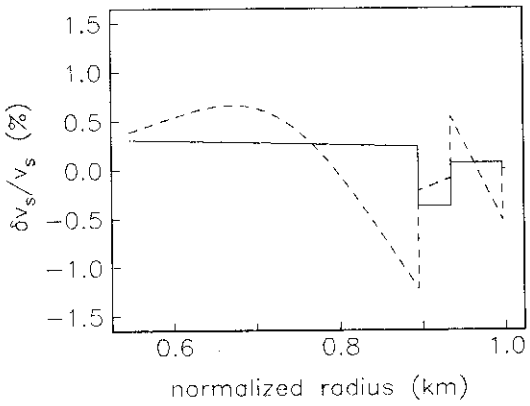

Fig. 19. Comparison between Y_2^0 mantle models expressed as relative perturbation in shear velocity generated with (solid line) and without (dashed line) the inclusion of aspherical boundary structure on the 400 and 670 km discontinuities. The c_2^0 coefficients are fit better without the large boundary perturbations, but this illustrates the formal trade-off between volumetric and boundary perturbations which troubles interpretation.

combination of real part Y_2^2 and Y_2^0 of opposite sign from Ms2 (Figure 22). This comes as no surprise since DW1 is poorly constrained in this region. However, comparisons must be performed over broad regions due to resolving widths certainly being no less than 500 km for the data we use here. For example, it is likely that our data have difficulty discriminating between the Y_2^0 parts of Ms2 and DW1 near the 670 km discontinuity. The two models are quite different qualitatively, one (DW1) with large negative structure confined to the transition zone and the other (Ms2) with the negative structure in the lower mantle. However, the averages over a region several hundred kilometers on either side of the discontinuity are approximately the same. Nevertheless, the systematic misfit to the c_2^0 coefficients for ${}_0S_{20}-{}_0S_{30}$ by DW1 in Figure 17 implies to us that at least some components of this Y_2^0 structure must be found in the lower mantle. We will pursue this further when we generalize spectral fitting to encompass coupled multiplets. The existence of a relatively large negative Y_2^0 structure near the top of the lower mantle can be constrained with the c_2^0 coefficients from ${}_0S_{10}-{}_0S_{19}$ which will result from this analysis.

We do not wish to interpret upper mantle structure due to the simplicity of its representation in Ms2, although there is qualitative agreement with DW1 (Figure 23). We also do not interpret Moho structure nor structure in the uppermost mantle due to trade-offs between these features. However, for comparison, Figure 18 exhibits the similarity between the Moho perturbation that we estimate and the Moho correction devised by *Woodhouse and Dziewonski* [1984]. The estimated Moho perturbation probably agrees with the Moho correction to within the uncertainty in the correction. We take the similarity between the inferred and the model Moho perturbations to indicate that it is not likely that crustal structure contaminates our model below the upper mantle. Since a great deal of interest has recently focused on CMB undulations, it may be worth noting that we estimate approximately 3 km of structure on the CMB and that its pattern is similar to

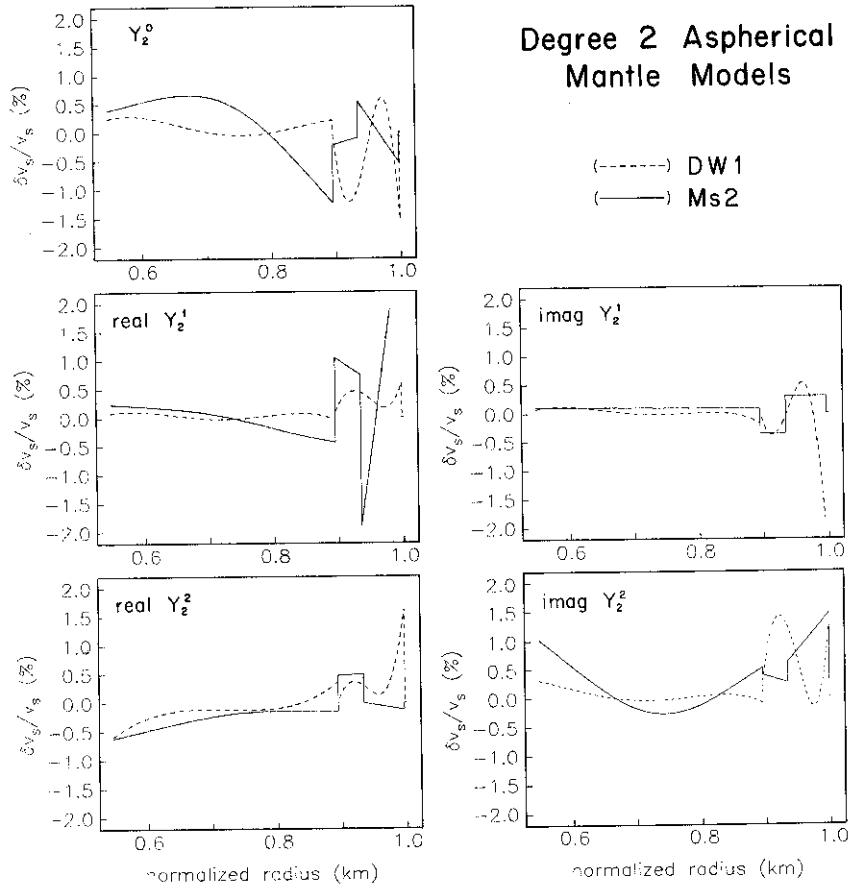

Fig. 20. Degree 2 mantle models expressed as a relative perturbation in shear velocity versus normalized radius in the mantle. The solid line is our model, Ms2, and the dashed line is DW1.

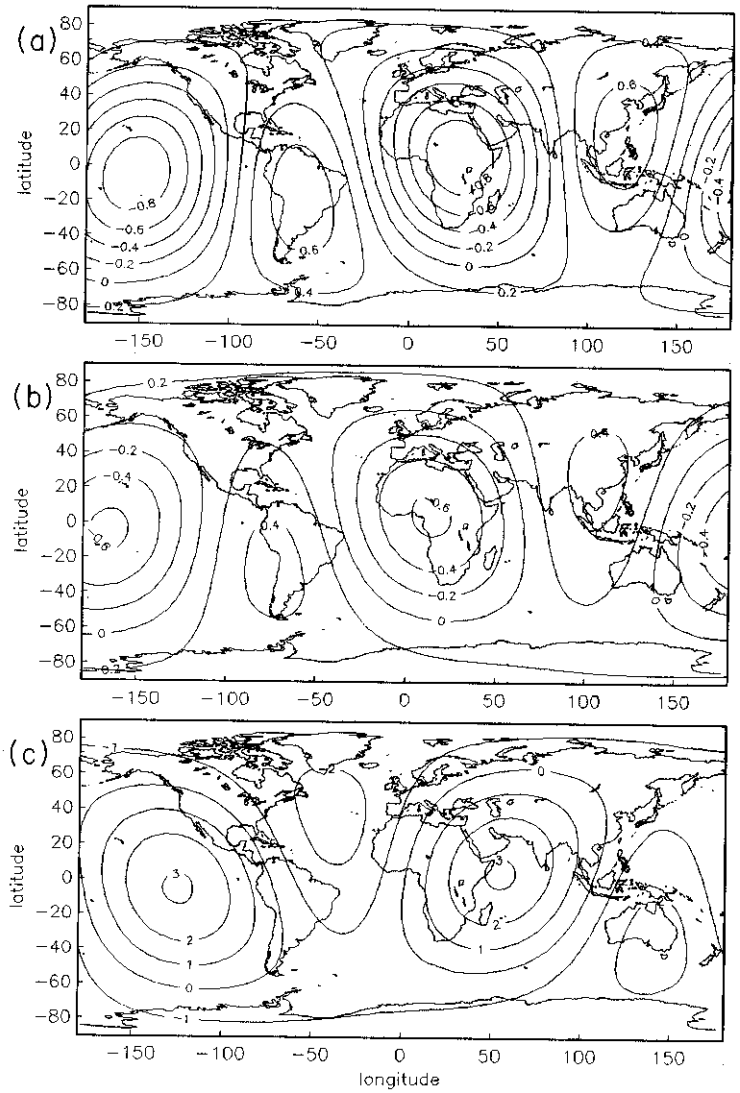

Fig. 21. Comparison between volumetric perturbations ($\delta v_s/v_s$ in %) in (*a*) our model Ms2 and (*b*) DW1 at 100 km above the CMB. (*c*) Estimated CMB perturbation (in kilometers) is also plotted for comparison.

lowermost mantle volumetric structure (Figure 21*c*). That is, depressions on the CMB appear to approximately underlie fast/dense lower mantle regions. For comparison with *Gwinn et al.* [1986] we note that the Y_2^0 components of the CMB undulation is approximately 1 km. However, the data could be fit by allowing this value to vary by several kilometers in either direction as long as the lowermost mantle is free to absorb more structure.

4.3. *Core Models*

Although Ms2 does not fit the nonaxisymmetric part of the anomalous multiplets perfectly, it goes a long way in that direction, and we feel that we are not warranted to infer anything about nonaxisymmetric core heterogeneity. However, the c_2^0 coefficients for the anomalous multiplets are extremely poorly fit by Ms2, as is shown in Figure 12*a*. Figure 12*a* shows the fit to all 38 c_2^0 estimates by Ms2. A cloud of observations, all for anomalous modes, with large observed c_2^0 values is very poorly fit. We seek a perturbation to core structure which increases all the model c_2^0 values, uniformly translating this cloud of points to the right to intersect the diagonal line. A great many types of models go part of the way to this end. Improvements can be achieved by the inclusion of any of the following structures: isotropic perturbations in the inner or outer core, boundary perturbations to the ICB and CMB, and also apparently anisotropic perturbations to the inner core [*Woodhouse et al.*, 1986]. The last structure is the only one on this list which appears to allow the very anomalously split but poorly excited multiplet ${}_3S_2$ to be fit. However, the amount of structure necessary in every case is sufficient to cause consternation by most. For example, *Ritzwoller et al.* [1986] argued that outer core structure is probably physically unrealistic, although they found that a simple outer core structure could be found to fit the singlet frequencies of most anomalous multiplets. It has, further, been suggested by *Giardini et al.* [1987] that structure in the top of the outer core, for example, in the form of a chemical boundary layer [*Creager and Jordan*, 1986*b*], can be dismissed on purely observational grounds citing the systematic misfitting it would cause for ${}_3S_1$ and ${}_2S_4$. This argument highlights the dependence of inferences about the core on a priori information about the mantle. Their argument is true if DW2 were the lower mantle model, but other lower mantle

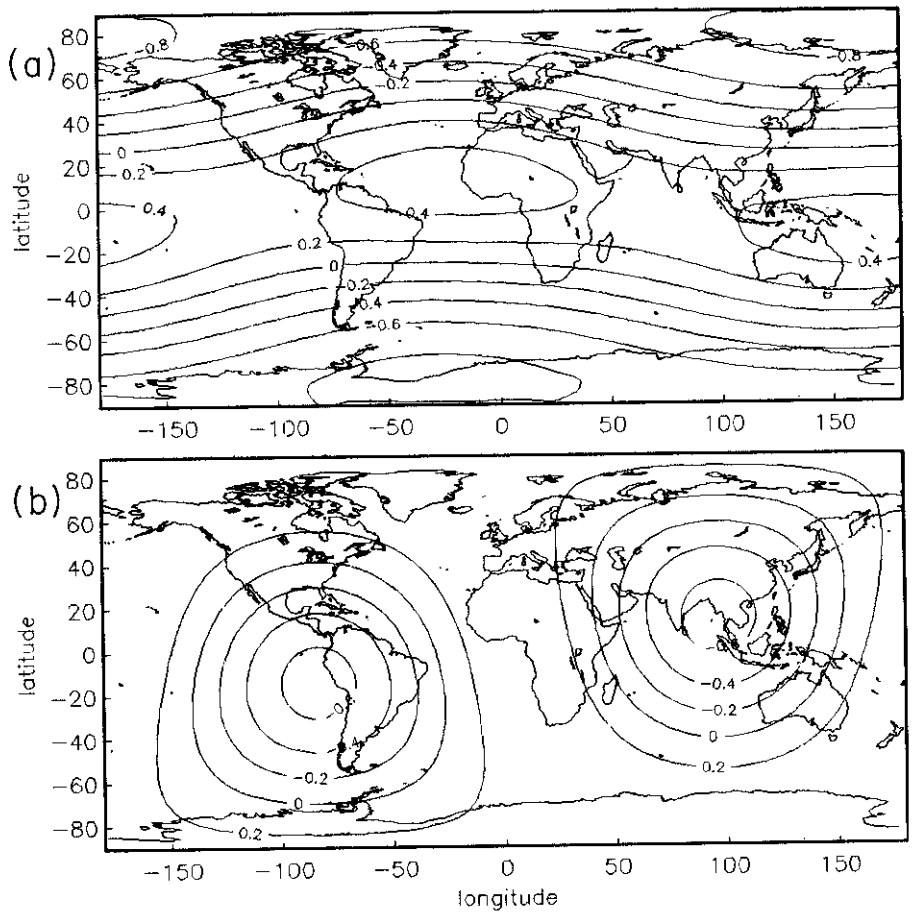

Fig. 22. Comparison between volumetric perturbations ($\delta v_s/v_s$ in %) in (*a*) our model Ms2 and (*b*) DW1 near the top of the lower mantle at 750 km depth. This is the region where these two models differ most appreciably.

models can be found which allow these two modes to be fit in the presence of outer core structure and still fit the remainder of the coefficients better than DW2. The question then reduces to how well these models fit the ISC data and other seismic data. This question continues to receive more work.

Independent of which mantle model one chooses, the anomalous multiplets are difficult to fit. For example, Figure 12*b* shows the fit in which 10 km of structure is on the ICB, 3 km on the CMB, and of the order of 1% lateral density variation in the inner core. Irrespective of the physical reasonableness of this model, many, but not all, of the coefficients are fit better. This is characteristic of most of the models we have considered to date with particular problems associated with fitting the c_2^0 coefficients of ${}_2S_3$ and ${}_3S_2$. Since a choice between competing models to explain the remaining anomalous multiplets would be ad hoc, we present no core model here. The resolution to the problem of anomalous splitting will await more and different data and confidence in the mantle part of the model.

It is interesting to note a parallel between core models for the present data set and core models of the underlying monopole. In a recent study, G. Masters and F. Gilbert (unpublished manuscript, 1987) used 350 degenerate frequency measurments to obtain better monopole models. They were able to reduce chi-square (χ^2) to a value of 500, but to achieve that value, it was necessary to allow the model to be transversely isotropic in all solid regions and to have additional discontinuities near the ICB and CMB. Sorting the modes on ray parameter ($p = (\ell+\frac{1}{2})/\omega$ is the ray parameter associated with a mode) revealed that 300 modes with $p > p_0$ had $\chi^2 = 350$ and 50 modes with $p < p_0$ had $\chi^2 = 150$, where $p_0 (= r_0/v_p(r_0))$ corresponds to the middle of the outer core. That is, mantle modes and modes sensitive to the upper outer core are acceptably well fit, but modes sensitive to the lower outer core and the inner core are very poorly fit.

An acceptable explanation of the results of modeling the monopole has not been presented, but the results give one pause when thinking about aspherical core models. If the monopole model is incorrect in its cores, then the eigenfunctions of its core sensitive modes may also be incorrect. Since these eigenfunctions are used as a basis for studying aspherical core models, it is possible that the difficulty in finding simple aspherical core models which fit the free oscillation data well and the difficulty in finding any monopole core model that acceptably fits the degenerate frequencies of the core sensitive modes are related.

5. SUMMARY AND CONCLUSIONS

Until recently, techniques devised to infer aspherical structure have been based on asymptotic formalisms which reduce, in essence, to the analysis of modal frequency (or temporal phase). A more nearly complete use of long-period data would include amplitude information as well. This study reports on the systematic application of one such technique to a number of low harmonic degree multiplets believed to be no more than weakly coupled to other nearby multiplets.

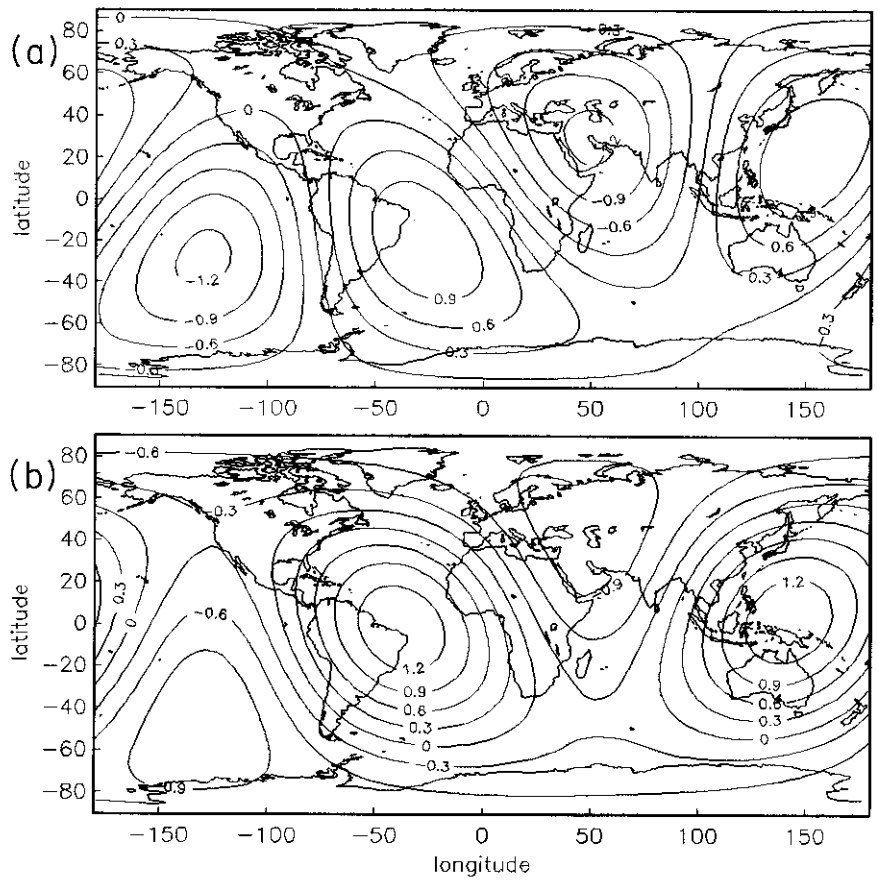

Fig. 23. Comparison between volumetric perturbations ($\delta v_s / v_s$ in %) in (*a*) our model Ms2 and (*b*) DW1 in the middle of the transition zone at 550 km depth.

For a multiplet genuinely isolated in complex frequency, the effect of even-order aspherical structure on the splitting matrix can be represented by a discrete set of complex coefficients. These coefficients determine the interaction between the singlets within the multiplet, and therefore we call them interaction coefficients. Together with a set of radial eigenfunctions computed from a spherical Earth model and an estimated moment tensor, the interaction coefficients completely represent the effect of aspherical structure on the seismic displacement field. The interaction coefficients can be estimated by iterative spectral fitting, a Newton's method technique the goal of which is to improve the coefficient estimates by minimizing the spectral residual. These coefficients linearly constrain aspherical structure and can be used as consistency checks on existing models or as data in inversions for aspherical structure, either by themselves or with other data. We applied iterative spectral fitting to approximatley 350 IDA and GDSN recordings taken from 18 large or deep events and estimated the degrees 2 and 4 interaction coefficients for 38 low harmonic degree ($\ell \leq 9$) multiplets, 28 of which are dominantly sensitive to the mantle and 10 of which are anomalous. The degree 2 mantle sensitive coefficients behave smoothly along the low radial order dispersion branches (${}_0S$, ${}_1S$, ${}_2S$, ${}_5S$), indicating that a smooth mantle model exists that will fit them. Synthetic experiments clearly demonstrate that representation errors (e.g., coupling, unspecified higher-order structure, errors in source mechanisms, errors in the radial eigenfunctions due to inaccurate spherical earth models, etc.) do perturb coefficient estimates and traditional error analyses produce overly optimistic error estimates. We present an error analysis, based on misfit, which appears to generate realistic error estimates. The estimated coefficients and errors are tabulated for use in future inversions. Since the degree 4 coefficients lie, on average, below the estimated errors, we do not interpret them.

Systematic misfit above ambient noise is symptomatic of errors in assumptions and approximations which can lead to biased coefficient estimates. Genuinely isolated mantle sensitive multiplets can be fit exceedingly well. Misfit to anomalous multiplets may primarily result from errors in the radial eigenfunctions. There are also difficulties in fitting the degenerate frequencies of the anomalous modes as well as other modes sensitive to core structure with spherical models. This result suggests that spherical core models are somehow in error, but an acceptable explanation has not yet been found. If the spherical model is incorrect in the core, then errors in the eigenfunctions computed from the model translate directly into errors in the interaction coefficients computed from aspherical models. If these errors are large, the interpretation of the estimated coefficients in terms of aspherical structure may be misleading.

Misfit to mantle sensitive multiplets is dominated by unspecified higher-order structure and coupling. At least for the multiplets considered here, the perturbing effect of higher-order structure on the estimated coefficients is relatively small. However, even weak coupling can greatly degrade coefficient estimates, implying that the estimation of accurate coefficients requires the judicious choice of candidate multiplets. Since the degradation in fit to the data for coupled multiples behaves in

accordance with expectations from synthetic experiments, the resultant errors are probably understood, and strongly coupled multiplets have been avoided. Although strong coupling vitiates the spectral fitting algorithm discussed here, it sensitizes the data to aspects of aspherical structure which genuinely isolated multiplets do not experience. For example, analysis of the misfit for the coupled pairs ${}_1S_5-{}_2S_4$ and ${}_1S_6-{}_2S_5$ indicates that they are coupling through odd degrees 1 and 3 of aspherical structure. However, synthetic experiments indicate that they are coupled less strongly than predicted by the upper mantle model M84A together with the lower mantle model LO2.56, leading us to hypothesize tentatively that these models are too large at degrees 1 and 3 in an integrated sense. The generalization of spectral fitting to encompass coupled modes is straightforward [*Ritzwoller*, 1987] and will be the subject of a later paper. A careful analysis of nearly equally excited overtones such as ${}_1S_5-{}_2S_4$ and ${}_1S_6-{}_2S_5$ should yield new constraints on odd-degree structure. Analysis of ${}_0S_{10}$ through ${}_0S_{22}$ which are strongly coupled to nearby toroidal modes by the Coriolis force should help resolve some of the ambiguities concerning the inference of structures in the neighborhood of the 400- and 670-km discontinuities.

Existing aspherical models have been represented as a single perturbation in radius, either v_s (M84A) or v_p (LO2.56). However, the computation of interaction coefficients from these models requires perturbations in v_s, v_p, and ρ simultaneously. A common approach to this problem has been to assume an empirical linear scaling law between relative perturbations in v_s, v_p, and ρ. Appropriate values of the scaling relationships in the deep Earth, especially $d \ln v_s / d \ln v_p$, are currently being debated. Errors in the scaling law translate into ambiguities in the amplitude of the aspherical model, exacerbating quantitative comparison with the estimated coefficients. Nevertheless, for comparison with existing models we are forced to use a scaling law approach. We consider the range of values for $d \ln v_s / d \ln v_p$ under debate (1.25–2.5) as end-members in a suite of physically realistic alternatives and report comparisons from both end-members. In either case, there is qualitative agreement along the ${}_0S$, ${}_1S$, ${}_2S$, and ${}_5S$ branches with the coefficients computed from M84A–LO2.56. The χ^2 of the $28\times5=140$ degree 2 coefficients for the mantle sensitive multiplets is 469 relative to M84A and LO2.56 with $d \ln v_s / d \ln v_p = 1.25$ and 328 for $d \ln v_s / d \ln v_p = 2.50$. Thus, as *Giardini et al.* [1987] point out, the agreement with the larger scaling ratio is improved. However, all the improvement comes only from a few coefficients (c_2^0 and Re (c_2^2) along the ${}_0S$ and ${}_1S$ branches) and can be accommodated as easily by extra structure at the base of the mantle or a CMB perturbation. Furthermore, the models still do not quantitatively fit the coefficients. Unless these structures can be safely ruled out, evidence for a high $d \ln v_s / d \ln v_p$ ratio is not unequivocal. With notable exceptions, the interaction coefficients for ${}_0S_{20}-{}_0S_{40}$ computed by *Smith et al.* [1987] from multiplet center frequency measurements agree fairly well with those predicted from M84A–LO2.56 regardless of scaling. Total misfit is not good; the $21\times5=105$ degree 2 coefficients for the surface wave multiplets with $d \ln v_s / d \ln v_p = 1.25$ have $\chi^2=831$ and have $\chi^2=1204$ for $d \ln v_s / d \ln v_p = 2.50$. Most of this χ^2 comes from the c_2^2 coefficients for modes with harmonic degrees less than 27. Fundamental modes with harmonic degrees below 27 strongly sample the top of the lower mantle, a region not well sampled by the compressional waves used in the construction of LO2.56. Thus it is not unlikely that a fairly large Y_2^0 structure exists near the top of the lower mantle which is not represented by M84A or LO2.56 but which does appear in our inversions. The analysis of ${}_0S_{10}$ through ${}_0S_{22}$ will constrain this structure further.

Since existing models do not fit the estimated coefficients quantitatively, it is interesting to inquire into the range of models which do fit the coefficients well. For this reason we present the result of an inversion for degree 2 mantle structure using a method of inversion quite different from that used in previous inversions for aspherical mantle models. We explicitly solve for smooth models between seismic discontinuities by minimizing the sum of the integral of the square of the radial second derivative of the volumetric perturbation and the square of the Euclidean norm of the boundary perturbations. We use $d \ln v_s / d \ln v_p = 1.25$ throughout the mantle, and the resulting model fits the data at the desired level: $\chi^2=111$ for the 140 mantle sensitive coefficients and $\chi^2=64$ for the 105 surface wave coefficients. However, trade-offs between volumetric perturbations and boundary perturbations seriously trouble the inversion. The inferred Moho undulation is quire similar to the degree 2 part of the Moho model created by *Woodhouse and Dziewonski* [1984]. However, since structure on the Moho and uppermost mantle structure trade-off and since the parameterization of our model is very crude in the upper mantle, we do not interpret uppermost mantle structure. Trade-offs between possible undulations on the 400- and 670-km discontinuities and uppermost mantle transition zone structure are less severe than for the Moho and uppermost mantle, since jumps in the seismic parameters across the deeper discontinuities are smaller than across the Moho. We assume that there are no first-order discontinuities at 400 and 670 km and solve only for volumetric perturbations in these regions. With this assumption, we get a fairly good qualitative agreement with M84A in the transition zone. A strong first-order discontinuity exists at the CMB, and we solve for it as well as lowermost mantle structure. In agreement with LO2.56, the lower mantle is dominated at most depths by Y_2^0 and Y_2^2 with most of the structure concentrated near the boundaries (CMB and 670 km). There is good qualitative agreement with LO2.56 in the lowermost mantle, but in the upper part of the lower mantle the models differ substantially where we infer a large negative Y_2^0 structure. We present a map of the CMB undulation but warn the reader that the data can be fit well without it.

The c_2^0 coefficients for the anomalous multiplets are extremely poorly fit by the mantle model and core structure is necessary to fit them. Many types of models go part of the way toward this end with improvements yielded by the following structures: isotropic perturbations in the inner or outer cores, boundary perturbations on the ICB and CMB, and also apparently anisotropic perturbations in the inner core [*Woodhouse et al.*, 1986]. The last structure is the only one on this list which appears to allow the most anomalously split, but poorly excited, mode ${}_3S_2$ to be fit. All the other anomalous modes can be fit with a combination of the other structures. Except in the form of boundary layers, outer core structure can probably be ruled out on theoretical grounds. *Giardini et al.* [1987] suggest that it can be ruled out on purely observational grounds citing the systematic misfit to ${}_3S_1$ and ${}_2S_4$ which it would produce. Their argument is true if LO2.56 were the lower mantle model and $d \ln v_s / d \ln v_p = 2.5$ throughout the lower mantle but, again, does not follow as long as perturbations can be put on the CMB or if the lowermost mantle were to differ from LO2.56. The modal data alone do not rule out core boundary layers and do not unequivocally establish a large $v_s : v_p$ scaling ratio.

With the generalization of the technique to a form applicable to

coupled modes, spectral fitting can be applied fruitfully to many more modes than we have analyzed here. The success of the technique should be marked by the data being fit extremely well; total variance reductions exceeding 80% for the genuinely isolated multiplets are not uncommon. If the fit to each coupled set of multiplets is as good as this, judgements of the quality of the results will be more straightforward and the resulting models more reliable.

APPENDIX: CONSTRUCTING SMOOTH MODELS BETWEEN DISCONTINUITIES

Consider a piecewise continuous reference Earth model comprising a set of D concentric shells ($r_d \le r \le r_{d+1}$) overlain by D boundaries $\{h_d : d = 1, ..., D\}$. Assuming that the interaction coefficients of different degrees and orders do not covary, the problem of inferring aspherical structure breaks into independent inversions for each degree s and order t. Therefore we can suppress these indices and rewrite the forward problem given by (9) as

$$c_k = \sum_{d=1}^{D} \left\{ \int_{r_d}^{r_{d+1}} G_k(r)\delta m(r)dr - h_{d+1\,k}D_{d+1} \right\} \tag{A1}$$

where

$$\begin{aligned} {}_kD_{d+1} &= {}_kB_{d+1}r_d^2 \\ \delta m(r) &= \delta v_s(r)/v_s(r) \\ G_k(r) &= \left\{ K_k(r)\kappa(r)\frac{d\ln\kappa}{d\ln v_s} + M_k(r)\mu(r)\frac{d\ln\mu}{d\ln v_s} \right. \\ &\quad \left. + R_k(r)\rho(r)\frac{d\ln\rho}{d\ln v_s} \right\} r^2 \end{aligned}$$

We call G_k the combined representer for multiplet k.

The partial derivatives of κ and μ with respect to v_s can be computed from (16) as follows:

$$\frac{d\ln\kappa}{d\ln v_s} = \frac{d\ln\kappa}{d\ln\rho}\left[\frac{d\ln v_s}{d\ln\rho}\right]^{-1} \approx 1.7$$

since

$$\frac{d\ln\kappa}{d\ln\rho} = 1 + \frac{2}{1-x}\frac{d\ln v_s}{d\ln\rho}\left[\frac{d\ln v_p}{d\ln v_s} - x\right] \approx 4.3$$

where $x = (2v_s/\sqrt{3}\,v_p)^2 \approx 0.4$ in the mantle.

$$\frac{d\ln\mu}{d\ln v_s} = \frac{d\ln\mu}{d\ln\rho}\left[\frac{d\ln v_s}{d\ln\rho}\right]^{-1} \approx 2.4$$

since

$$\frac{d\ln\mu}{d\ln\rho} = 1 + 2\frac{d\ln v_s}{d\ln\rho} \approx 6.0$$

The estimation of $\delta m(r)$ and $\{h_d\}_{d=1}^{D}$ is a function of the choice of norm to optimize. There are many variations on this theme, but one fruitful approach [*Gilbert et al.*, 1973] is to construct smooth models between discontinuities by minimizing the sum of the integral of the square of the radial second derivative of $\delta m(r)$ and the square of the Euclidean norm of the boundary vector $\mathbf{h} = (h_1, ..., h_D)^T$. That is, we minimize N where

$$N = \sum_d \left\{ w_d \int_{r_d}^{r_{d+1}} (\delta m''(r))^2 dr + \lambda_d h_d^2 \right\} \tag{A2}$$

and where $\delta m''$ is the second radial derivative of δm and λ and w are suitably chosen boundary and layer weights, respectively, which for simplicity we now choose to be unity. For clarity, we can consider a single shell (r_d, r_{d+1}) and overlying boundary h_{d+1} and temporarily drop the summation in (A1) and (A2).

In practice, to minimize N, we first integrate (A1) by parts twice to produce a forward problem in $\delta m''$. The minimum norm solution can then be obtained in the standard way [*Parker*, 1977]. (It is easy to verify that N is minimized by expanding $\delta m''$ in $G_k(r)$ with the result then being resubstituted into (A1) to be solved for the expansion coefficients.) The details follow.

Integrating (A1) by parts twice yields

$$\begin{aligned} c_k &= \delta m(r_d)F_k(r_d) + \delta m'(r_d)R_k(r_d) \\ &\quad + \int_{r_d}^{r_{d+1}} G_k(r)\delta m''(r)dr - h_{d+1\,k}D_{d+1} \end{aligned} \tag{A3}$$

where F_k and R_k are the partial layer integrals

$$F_k(r) = \int_r^{r_{d+1}} G_k(r')dr'$$

$$R_k(r) = \int_r^{r_{d+1}} F_k(r')dr'$$

Note that $F_k(r_d)$ and $R_k(r_d)$ in (A3) are the complete layer integrals. Now let

$$\begin{aligned} \delta m(r_d) &= \sum_{k'} \alpha_{k'} F_{k'}(r_d) \\ \delta m'(r_d) &= \sum_{k'} \beta_{k'} R_{k'}(r_d) \\ \delta m''(r) &= \sum_{k'} \gamma_{k'} G_{k'}(r) \\ h_{d+1} &= \sum_{k'} \delta_{k'\,k} D_{d+1} \end{aligned} \tag{A4}$$

so that (A3) becomes

$$c_k = \sum_{k'} \mathbf{y}_{k'} \cdot \mathbf{X}_{kk'} \tag{A5}$$

where $\mathbf{y}_k$ is the coefficient vector for multiplet k

$$\mathbf{y}_k = (\alpha_k, \beta_k, \gamma_k, \delta_k)^T$$

and $\mathbf{X}_{kk'}$ is the Gram matrix

$$\mathbf{X}_{kk'} = (F_k F_{k'}, R_k R_{k'}, \Gamma_{kk'}, D_k D_{k'})^T$$

where Γ is

$$\Gamma_{kk'} = \int_{r_d}^{r_{d+1}} G_k(r)G_{k+1}(r)dr$$

Equation (A5) can be "solved" for $\mathbf{y}_k$ and hence $\delta m(r_d)$, $\delta m'(r_d)$, and $\delta m''(r)$ for $r\varepsilon(r_d, r_{d+1})$ by (A4). The model $\delta m(r)$ can then be reconstructed with the following equations:

$$\begin{aligned} \delta m(r_1) &= \delta m(r_d) \\ \delta m'(r_1) &= \delta m'(r_d) \\ \delta m(r_{j+1}) &= \delta m(r_j) + (r_{j+1}-r_j)\delta m'(r_j) \\ &\quad + \tfrac{1}{2}(r_{j+1}-r_j)^2\delta m''(r_j) \end{aligned} \tag{A6}$$

where $\{r_j\}_{j=1}^{J}$ is an ordered sequence of radii on (r_d, r_{d+1}) such that $r_j \le r_{j+1}$ for all j. The final equation in (A6) is simply a recurrence relation based on a truncated Taylor series with the first two equations being the required initial conditions. A model constructed from (A6) must at least be smooth in the sense that all radial derivatives higher than the second vanish. In practice, the smoothness of the model is a function of the number of eigenvalues retained in the decomposition of **X**. We seek models, such as Ms2, which are very smooth between discontinuities and keep a small fraction of the eigenvalues.

The sum over shells can be retrieved by simply adding Σ_d in (A3) and following the algebra as before.

Acknowledgments. We are very grateful for the high-quality digital data provided to us by the IDA and GDSN organizations. We would like to thank J. Park for allowing us to use his modal coupling code and I. Henson for running it in the synthetic experiments. We would also like to thank R. Widmer for editing some of the data and computing the moment tensors for a number of events and F. Dahlen for his review. This research has been supported by National Science Foundation grants EAR-84-10369 and EAR-84-18471.

REFERENCES

Buland, R., D. Yuen, K. Konstanty, and R. Widmer, Source phase shift: A new phenomenon in wave propagation due to anelasticity, *Geophys. Res. Lett., 12*(9), 569–572, 1985.

Chung, D. H., Elasticity and equations of state of olivines in the Mg_2SiO_4–$FeSiO_4$ system, *Geophys. J. R. Astron. Soc., 25*, 511–538, 1971.

Clayton, R. W., and R. P. Comer, A tomographic analysis of mantle heterogeneities from body wave travel times (abstract), *Eos Trans. AGU, 64*, 776, 1983.

Creager, K., and T. Jordan, Slab penetration into the lower mantle beneath the Mariana and other island arcs of the northwest Pacific, *J. Geophys. Res., 91*, 3573–3589, 1986*a*.

Creager, K., and T. Jordan, Aspherical structure of the core-mantle boundary from *PKP* travel times, *Geophys. Res. Lett., 13*(13), 1497–1500, 1986*b*.

Dahlen, F. A., and R. V. Sailor, Rotational and elliptical splitting of the free oscillations of the Earth, *Geophys. J. R. Astron. Soc., 58*, 609–623, 1979.

Davis, J. P., Local eigenfrequency and its uncertainty from fundamental spheroidal mode frequency shifts, *Geophys. J. R. Astron. Soc., 88*, 693–722, 1987.

Davis, J. P., and I. M. Henson, Validity of the great circular average approximation for inversion of normal mode measurements, *Geophys. J. R. Astron. Soc., 85*, 69–92, 1986.

Doornbos, D., Present seismic evidence for a boundary layer at the base of the mantle, *J. Geophys. Res., 88*, 3499–3505, 1983.

Dziewonski, A. M., Mapping the lower mantle: Determination of lateral heterogeneity in *P* velocity up to degree and order 6, *J. Geophys. Res., 89*, 5929–5952, 1984.

Edmonds, A. R., *Angular Momentum and Quantum Mechanics*, Princeton University Press, Princeton, N. J., 1960.

Giardini, D., X.-D. Li, and J. Woodhouse, Three dimensional structure of the Earth from splitting in free oscillation data, *Nature, 325*, 405–409 1987.

Gilbert, F., and A. M. Dziewonski, An application of normal model theory to the retrieval of structural parameters and source mechanisms from seismic spectra, *Philos. Trans. R. Soc. London, Ser. A, 278*, 187–269, 1975.

Gilbert. F., A. M. Dziewonski, and J. Brune, An informative solution to a seismological inverse problem, *Proc. Natl. Acad. Sci. U.S.A., 70*, 1410–1413, 1973.

Golub, G., and C. Reinsch, Singular value decompositions and least squares solutions, in *Linear Algebra*, edited by J. H. Wilkinson and C. Reinsch, pp. 134–151, Springer-Verlag, New York, 1971.

Gwinn, C., T. Herring, and I. Shapiro, Geodesy by radio interferometry: Studies of the forced nutations of the Earth, 2, Interpretation, *J. Geophys. Res., 91*, 4755–4765, 1986.

Hager, B. H., Subducted slabs and the geoid: Constraints on mantle rheology and flow, *J. Geophys. Res., 89*, 6003–6015, 1984.

Hales, A. L., and H. A. Doyle, *P* and *S* travel time anomalies and their interpretation, *Geophys. J. R. Astron. Soc., 13*, 403–415, 1967.

Huber, P., *Robust Statistics*, John Wiley, New York, 1981.

Ito, E., and H. Yamada, Stability relations of silicate spinels, ilmenites, and perovskites, in *High Pressure Research in Geophysics*, edited by S. Akimoto and M. H. Manghnani, pp. 405–419, Center for Academic Publications, Tokyo, Japan, 1982.

Jarvis, G. T., and W. R. Peltier, Lateral heterogeneity in the convecting mantle, *J. Geophys. Res., 91*, 435–451, 1986.

Jordan, T. H., A procedure for estimating lateral variations from low-frequency eigenspectra data, *Geophys. J. R. Astron. Soc., 52*, 441–455, 1978.

Jordan, T. H., and W. S. Lynn, A velocity anomaly in the lower mantle, *J. Geophys. Res., 79*, 2679–2684, 1974.

Lawson, C., and R. Hanson, *Solving Least Squares Problems*, Prentice Hall, Englewood Cliffs, N. J., 1974.

Lay, T. Structure of the Earth: Mantle and core, *Rev. Geophys., 25*, 1161–1167, 1987.

Lerch, F. J., S. M. Klosko, G. B. Patel, and C. A. Wagner, A gravity model for crustal dynamics (GEM-L2), *J. Geophys. Res., 90*, 9301–9311, 1985.

Liu, L., On the 650 km seismic discontinuity, *Earth Planet. Sci. Lett., 42*, 202–208, 1979.

Masters, G., and F. Gilbert, Structure of the inner core inferred from observations of its spheroidal shear modes, *Geophys. Res. Lett., 8*(6), 569–571, 1981.

Masters, G., and F. Gilbert, Attenuation in the Earth at low frequencies, *Philos. Trans. R. Soc. London, Ser. A, 308*, 479–522, 1983.

Masters, G., and M. Ritzwoller, Low frequency seismology and three-dimensional structure—Observational aspects, in *Mathematical Geophysics, A Survey of Recent Developments in Seismology and Geodynamics*, edited by N. J. Vlaar, G. Nolet, M. J. R. Wortel, and S. A. P. L. Cloetingh, pp. 1–30, Reidel, Hingham, Mass., 1987.

Masters, G., T. H. Jordan, P. G. Silver, and F. Gilbert, Aspherical Earth structure from fundamental spheroidal-mode data, *Nature, 298*, 609–613, 1982.

Masters, G., J. Park, and F. Gilbert, Observations of coupled spheroidal and toroidal modes, *J. Geophys. Res., 88*, 10,285–10,298, 1983.

Mauk, F. J., A teetonic based Rayleigh wave group velocity model for prediction of dispersion characteristic through ocean basins, Ph.D. thesis, Univ. of Mich., Ann Arbor, 1977.

Morelli, A., and A. Dziewonski, Topography of the core-mantle boundary and lateral heterogeneity of the liquid core, *Nature, 325*, 678–683, 1987.

Morelli, A., A. Dziewonski, and J. Woodhouse, Anisotropy of the inner core inferred from *PKIKP* travel times, *Geophys. Res. Lett., 13*(13), 1545–1548, 1986.

Okal, E. A., The effect of intrinsic ocean upper-mantle heterogeneity on regionalization of long-period Rayleigh wave phase velocities, *Geophys. J. R. Astron. Soc., 49*, 357–370, 1977.

Orcutt, J. A., K. M. Toy, and A. H. Olson, *P*- and *S*-wave station corrections: Results, isostatic modeling and gain correlation (abstract), *Eos Trans. AGU, 67*, 1114, 1986.

Parker, R. L., Understanding inverse theory, *Annu. Rev. Earth Planet. Sci., 5*, 35–64, 1977.

Poupinet, G., R. Pillet, and A. Souriau, Possible heterogeneity of the Earth's core deduced from *PKIKP* travel times, *Nature, 305*, 204–206, 1983.

Ringwood, A. E., *Composition and Petrology of the Earth's Mantle*, McGraw-Hill, New York, 1975.

Ritzwoller, M., Observational constraints on the large scale aspherical structure of the deep Earth, Ph.D. thesis, Univ. of Calif., San Diego, La Jolla, 1987.

Ritzwoller, M., and G. Masters, The fine structure of resolvably split multiplets (abstract), *Eos Trans. AGU, 65*, 1003, 1984.

Ritzwoller, M., G. Masters, and F. Gilbert, Observations of anomalous splitting and their interpretation in terms of aspherical structure, *J. Geophys. Res., 91*, 10,203–10,228, 1986.

Romanowicz, B. A., and M. Cara, Reconsideration of the relations

between S and P station anomalies in North America, *Geophys. Res. Lett.*, *7*, 417–420, 1980.

Silver, P. G., R. W. Carlson, P. Bell, and P. Olson, Mantle structure and dynamics, *Eos Trans. AGU*, *66*, 1193–1198, 1985.

Smith, M., G. Masters, and M. Ritzwoller, Constraining aspherical structure with normal mode frequency and attenuation measurements (abstract), *Eos Trans. AGU*, *68*, 358, 1987.

Souriau, A., and J. H. Woodhouse, A worldwide comparison of predicted S-wave delays from a three-dimensional upper mantle model with P-wave station correction, *Phys. Earth Planet. Inter.*, *39*, 75–88, 1985.

Stark, P. B., R. L. Parker, G. Masters, and J. A. Orcutt, Strict bounds on seismic velocity in the aspherical Earth, *J. Geophys. Res.*, *91*, 13,892–13,902, 1986.

Woodhouse, J. H., and F. A. Dahlen, The effect of a general aspherical perturbation on the free oscillations of the Earth, *Geophys. J. R. Astron. Soc.*, *53*, 335–354, 1978.

Woodhouse, J. H., and A. M. Dziewonski, Mapping the upper mantle: Three-dimensional modeling of Earth structure by inversion of seismic waveforms, *J. Geophys. Res.*, *89*, 5953–5986, 1984.

Woodhouse, J. H., and A. M. Dziewonski, Three dimensional mantle models based on mantle wave and long period body wave data (abstract), *Eos Trans. AGU*, *67*, 307, 1986.

Woodhouse, J. H., and D. Giardini, Inversion for the splitting function of isolated low order normal mode multiplets (abstract), *Eos Trans. AGU*, *66*, 300, 1985.

Woodhouse, J. H., and T. P. Girnius, Surface waves and free oscillations in a regionalized Earth model, *Geophys. J. R. Astron. Soc.*, *68*, 653–673, 1982.

Woodhouse, J., D. Giardini, and X.-D. Li, Evidence for inner core anisotropy from splitting in free oscillation data, *Geophys. Res. Lett.*, *13*(13), 1549–1552, 1986.

Yagi, T., P. M. Bell, and H.-K. Mao, Phase relations in the system MgO-FeO-SiO_2 between 150 and 700 kbar at 1000°C, *Year Book Carnegie Inst. Washington*, *78*, 614–618, 1979.

F. Gilbert and G. Masters, Institute of Geophysics and Planetary Physics, A-025, University of California, San Diego, La Jolla, California 92093.

M. Ritzwoller, Department of Earth and Planetary Sciences, Harvard University, Cambridge, MA 02138.

(Received April 22, 1987;
revised January 28, 1988;
accepted June 29, 1987.)